Atmospheric
Chemistry
and Physics

The influence of snow grain size and impurities on the vertical profiles of actinic flux and associated NO$_x$ emissions on the Antarctic and Greenland ice sheets

M. C. Zatko[1], T. C. Grenfell[1], B. Alexander[1], S. J. Doherty[2], J. L. Thomas[3,4], and X. Yang[5,6]

[1]Department of Atmospheric Sciences, Box 351640, University of Washington, Seattle, WA 98195, USA
[2]Joint Institute for the Study of Atmosphere and Ocean, 3737 Brooklyn Ave NE, Seattle, WA 98195, USA
[3]UPMC Univ. Paris 06, UMR8190, CNRS/INSU – Université Versailles St.-Quentin, LATMOS-IPSL, Paris, France
[4]Department of Atmospheric and Oceanic Sciences, University of California, Los Angeles, CA 90095, USA
[5]National Centre for Atmospheric Science (NCAS), Cambridge, CB2 1EW, UK
[6]Centre for Atmospheric Science, Department of Chemistry, University of Cambridge, Cambridge CB2 1EW, UK

Correspondence to: B. Alexander (beckya@atmos.washington.edu)

Abstract. We use observations of the absorption properties of black carbon and non-black carbon impurities in near-surface snow collected near the research stations at South Pole and Dome C, Antarctica, and Summit, Greenland, combined with a snowpack actinic flux parameterization to estimate the vertical profile and e-folding depth of ultraviolet/near-visible (UV/near-vis) actinic flux in the snowpack at each location. We have developed a simple and broadly applicable parameterization to calculate depth and wavelength dependent snowpack actinic flux that can be easily integrated into large-scale (e.g., 3-D) models of the atmosphere. The calculated e-folding depths of actinic flux at 305 nm, the peak wavelength of nitrate photolysis in the snowpack, are 8–12 cm near the stations and 15–31 cm away (>11 km) from the stations. We find that the e-folding depth is strongly dependent on impurity content and wavelength in the UV/near-vis region, which explains the relatively shallow e-folding depths near stations where local activities lead to higher snow impurity levels. We calculate the lifetime of NO$_x$ in the snowpack interstitial air produced by photolysis of snowpack nitrate against wind pumping ($\tau_{\text{wind pumping}}$) from the snowpack, and compare this to the calculated lifetime of NO$_x$ against chemical conversion to HNO$_3$ (τ_{chemical}) to determine whether the NO$_x$ produced at a given depth can escape from the snowpack to the overlying atmosphere. Comparison of $\tau_{\text{wind pumping}}$ and τ_{chemical} suggests efficient escape of photoproduced NO$_x$ in the snowpack to the overlying atmosphere throughout most of the photochemically active zone. Calculated vertical actinic flux profiles and observed snowpack nitrate concentrations are used to estimate the potential flux of NO$_x$ from the snowpack. Calculated NO$_x$ fluxes of 4.4×10^8–3.8×10^9 molecules cm^{-2} s^{-1} in remote polar locations and 3.2–8.2×10^8 molecules cm^{-2} s^{-1} near polar stations for January at Dome C and South Pole and June at Summit suggest that NO$_x$ flux measurements near stations may be underestimating the amount of NO$_x$ emitted from the clean polar snowpack.

1 Introduction

Research over the past two decades has provided ample evidence that unique photochemical reactions occur in snow-covered regions during periods of sunlight (Domine and Shepson, 2002; Grannas et al., 2007 and references within; Honrath et al., 1999). The photolysis of chemical species present in the snowpack, such as nitrate (NO$_3^-$), hydrogen peroxide (H$_2$O$_2$), formaldehyde (CH$_2$O), and nitrous acid (HONO), is a source of oxidants (OH, O$_3$, HO$_2$) to the atmosphere within and above the snowpack (Beine et al., 2002; Beyersdorf et al., 2007; Cotter et al., 2003;

Davis et al., 2001, 2004; Dibb et al., 2002; France et al., 2011; Frey et al., 2009; Honrath et al., 1999, 2002; Jones et al., 2001, 2011; Mauldin et al., 2010; Oncley et al., 2004; Sjostedt et al., 2007). Photochemical reactions in the snowpack have significant implications for the oxidizing capacity of the boundary layer over snow-covered regions (Chen et al., 2007; Grannas et al., 2007 and references within; Sjostedt et al., 2007; Thomas et al., 2012) and for the preservation of trace species such as H$_2$O$_2$ and NO$_3^-$ in ice cores (Lamarque et al., 2011; Mulvaney et al., 1998).

The formation and deposition of atmospheric nitrate (particulate NO$_3^-$ and HNO$_3$(g)) is typically thought to be a permanent sink for gaseous NO$_x$ (NO$_x$ = NO and NO$_2$) in the troposphere because gas-phase nitric acid (HNO$_3$(g)) is not readily photolyzed at wavelengths (λ) >325 nm (Johnston and Graham, 1973). However, nitrate deposited to the snowpack can be re-released to the atmosphere both by photolysis (as NO$_x$) (Davis et al., 2008; Honrath et al., 1999, 2002) and evaporation (as HNO$_3$) (Mulvaney et al., 1998) at depths below the snow surface followed by re-deposition to the surface snowpack (Rothlisberger et al., 2000). This is supported by observations of surface snow nitrate concentrations roughly an order of magnitude larger than nitrate concentrations at 10 cm depth in continental Antarctica snowpack (Dibb et al., 2004; Frey et al., 2009; Mayewski and Legrand, 1990; Rothlisberger et al., 2000) and by observations of an upward flux of NO$_x$ out of the snowpack in polar regions on the order of 1.3–6.7 × 10^8 molec cm^{-2} s^{-1} (Beine et al., 2002; Davis et al., 2004; Honrath et al., 1999; Jones et al., 2001; Oncley et al., 2004). The results of earlier isotopic (δ^{15}N) studies disagree on whether evaporation or photodenitrification is the dominant process of nitrate removal from the snowpack (Blunier et al., 2005; Savarino et al., 2007), but results from Frey et al. (2009) and Erbland et al. (2012) suggest that photodenitrification is the dominant contributor to post-depositional processing of NO$_3^-$ in East Antarctica (Dome C). The dominance of photodenitrification is consistent with observations of downward fluxes of HNO$_3$ to the snowpack (Dibb et al., 2004). Although both NO$_x$ and HONO are produced from NO$_3^-$ photolysis, observations of the upward flux of NO$_x$ above the snow surface at Summit, Greenland, were roughly an order of magnitude larger than the measured flux of HONO (Dibb et al., 2004). Factors such as snow accumulation rate, snow acidity, and the gradient of temperature within the snow may influence the redistribution of snowpack nitrate (Rothlisberger et al., 2000).

Several process-based modeling studies have calculated the flux of NO$_x$ from the high-latitude snowpacks at Neumayer, Antarctica (Wolff et al., 2002), Ny-Ålesund, Svalbard (France et al., 2010), Summit, Greenland (Thomas et al., 2011), Dome C, Antarctica (France et al., 2011), and Barrow, Alaska (France et al., 2012). Estimates of depth-integrated snowpack actinic flux are required to model the flux of NO$_x$ from the snowpack, where actinic flux is defined as the irradiance impingent through a given point in all (4π) directions.

Using surface irradiances from the British Antarctic Survey radiative transfer model (Gardiner and Martin, 1997) and a snowpack radiative transfer model (Grenfell, 1991), Wolff et al. (2002) calculated an e-folding depth of actinic flux in snowpack (z_e) of 3.7 cm at $\lambda = 320$ nm, where z_e is defined as the depth in the snowpack where the actinic flux is 1/e of the surface value (Warren et al., 2006). This e-folding depth is now thought to be too shallow, and measured and calculated z_e from later studies range from 6–9 cm at Ny-Ålesund, 10–20 cm at Dome C, and to 9–14 cm at Barrow (France et al., 2010, 2011, 2012).

Snowpack z_e values are dependent upon snow physical and optical properties (e.g., grain size, bulk density, refractive index) as well as the type and concentration of impurities in the snow (e.g., black carbon). Snow albedo is also dependent upon snow physical and optical properties, which is highlighted in a recent study by Carmagnola et al. (2012). Pure ice is a moderate absorber of near-infrared and a strong absorber of infrared radiation, but an extremely weak absorber of ultraviolet (UV) radiation, the latter of which is relevant for photochemistry. At UV and near-UV wavelengths, snow grains are much more efficient scatterers than absorbers; however, multiple scattering of radiation in the snowpack increases the probability of absorption by ice grains and impurities in the snow. Because ice is so weakly absorbing at these wavelengths, the absorption in natural snow is dominated by impurities, even in the cleanest snow. Dust, brown carbon, and humic-like substances (HULIS) also absorb radiation and have a much stronger wavelength dependence across the ultraviolet/near-visible (UV/near-vis) compared to black carbon (BC) (France et al., 2011, 2012; Hoffer et al., 2006). However, while the optical properties of HULIS have been estimated in several studies (France et al., 2012; Hoffer et al., 2006; Kirchsetter et al., 2004; Roden et al., 2006; Voisin et al., 2012), the range of optical properties for HULIS is large. Also, the amount of HULIS in the Arctic and Antarctic snowpack has only been quantified in one recent study (Voisin et al., 2012).

Since snow impurities dominate absorption in the UV/near-vis λ range, here we use optical measurements of particulate material collected on filters through which snow meltwater has been passed. We incorporate these impurity measurements into a simple parameterization to calculate depth-dependent actinic flux profiles in deep snowpack for λ between 289–850 nm in order to estimate the flux of NO$_x$ from the snowpack via NO$_3^-$ photolysis. The parameterization is derived (in Sect. 2.3 below) from a well-tested discrete-ordinate-method radiative transfer model for optically thick snow and ice (Grenfell, 1991), and can easily be incorporated into large-scale models such as global climate models and global chemical transport models. To estimate photolysis in the snow, we calculate the depth profile of actinic flux using the parameterization and our observations of the absorption properties of snow. We use the actinic flux parameterization to evaluate the sensitivity of the e-folding

Table 1. Description of snow samples collected near Dome C, Antarctica, in January 2004 and Summit, Greenland, in June 2007. The average and standard deviation (1σ) of black carbon concentration (C_{BC}), the Angstrom exponent (Å), the mean fraction of nonBC (f_{nonBC}) absorption in the $\lambda = 650$–700 nm and $\lambda = 298$–345 nm ranges, the snow depths over which these samples were collected, and the number of snow samples (n) collected at each location are provided. Please see Appendix B for more information about each sample collected.

Distance from station (km)	C_{BC} (ng g^{-1})	Å	$f_{nonBC\_650-700}$ (%)	$f_{nonBC\_298-345}$ (%)	Depth (cm)	n
Dome C, Antarctica						
< 0.5	2.1 ± 1.3	2.3 ± 0.4	20.0 ± 4.2	85.6 ± 2.9	0–20	13
11	0.6 ± 0.2	2.9 ± 0.4	29.0 ± 0.8	88.6 ± 0.8	0–20	4
Summit, Greenland						
20–40	1.4 ± 0.3	2.7 ± 0.3	29.0 ± 4.9	89.2 ± 2.2	0–90	5

depth to ice grain size (effective grain radius), wavelength, solar zenith angle, and snowpack BC and non-black carbon (nonBC) concentrations at $\lambda = 305$ nm. Results from the parameterization suggest that actinic flux is significant at depths greater than 1.5 m in the snow. We evaluate the assumption made in previous studies (France et al., 2010, 2011, 2012; Wolff et al., 2002) that all NO$_x$ produced in the snowpack will be ventilated to the overlying atmosphere by comparing the calculated depth-dependent lifetime of NO$_x$ in the snowpack interstitial air against physical and chemical sinks. The calculated actinic flux profile is integrated over snow depth and wavelength to compute the total flux of NO$_x$ from the snowpack, F_{NO_x}. Our calculated F_{NO_x} is compared to observations from inland sites in Antarctica and Greenland.

2 Methods

2.1 BC and nonBC absorption from filter samples

The amount of absorption from BC and nonBC material in the snowpack must be known to calculate the actinic flux profile using our parameterization. In this study, the amount of BC and nonBC absorption is estimated from optical measurements of impurities from snow collected on filters. Snow samples were collected for impurities in January 2004 at sites < 0.5 to 11 km from Dome C Station in Antarctica, and in June 2007 at sites 20–40 km from Summit Station in Greenland (see Table 1). The snow samples were processed in the field. Each sample was melted and filtered through a 0.4 μm Nuclepore filter to extract the particulate material in the meltwater. A maximum of 10 % of the particulate matter in the snow sample is lost during filtering. The filters were transported back to the University of Washington where the optical properties of the filters were measured using the ISSW spectrophotometer as described in Grenfell et al. (2011). The ISSW spectrophotometer uses an integrating sphere and integrating sandwich technique to determine the absorption spectrum in units of optical depth, $T(\lambda)$ (dimensionless, e.g., cm^2 cm^{-2}), from $\lambda = $300-750 nm of particu-
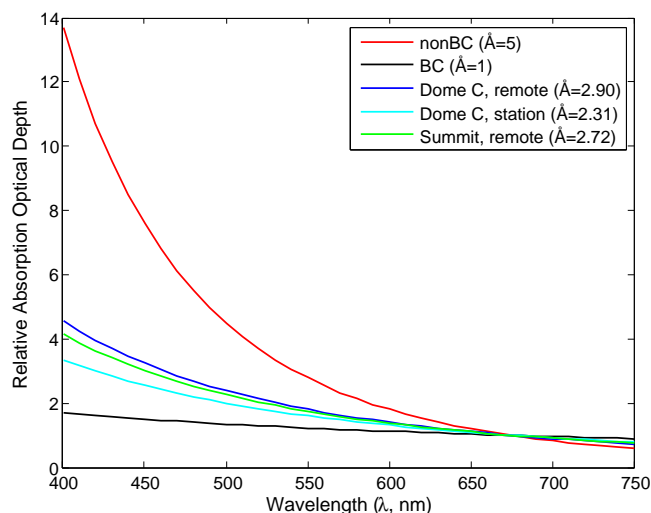

Fig. 1. Idealized absorption profiles (expressed in absorption optical depth, $T(\lambda)$) of BC (black) and nonBC (red) material from Grenfell et al. (2011) and Hoffer et al. (2006). Also shown are absorption profiles of snow samples collected in remote Dome C (blue), remote Summit (green), and near-station Dome C (cyan).

late material on filters while removing losses from scattering by the filter and the collected aerosols (Grenfell et al., 2011).

The spectral absorption measured by the spectrophotometer for each filter is conventionally characterized by an Ångström exponent (Å$_{tot}$) associated with the absorption of total (BC + nonBC) impurities on each filter between two visible wavelengths (λ_1 and λ_2) according to the formula

$$\text{Å}_{tot}(\lambda_1 \text{ to } \lambda_2) = \frac{\ln\left(\frac{T_{tot}(\lambda_1)}{T_{tot}(\lambda_2)}\right)}{\ln\left(\frac{\lambda_2}{\lambda_1}\right)}, \qquad (1)$$

where the total optical depth, $T_{tot}(\lambda)$, describes the absorption of all the impurities on each filter at a given λ. A larger Ångström exponent indicates a greater absorption at shorter wavelengths (Fig. 1), resulting in a more brownish color for the sample.

Measured $Å_{tot}$ from $\lambda = 450$–600 nm is used together with the assumed values of $Å_{BC} = 1$ and $Å_{nonBC} = 5$ (Doherty et al., 2010, and references within) to determine the fraction of absorption from $\lambda = 450$–600 nm due to BC impurities ($f_{BC\_450-600}$) from the relation

$$Å_{tot} = Å_{BC} \cdot f_{BC\_450-600}(\lambda_o) + Å_{nonBC}(1 - f_{BC\_450-600}(\lambda_o)), \quad (2)$$

where $\lambda_o = 525$ nm. Since the absorption of radiation by BC is relatively constant with wavelength, $f_{BC\_450-600}$ is used to determine the fraction of absorption due to BC in the $\lambda = 650$–700 nm range ($f_{BC\_650-700}$), where BC is the dominant absorber of radiation (Grenfell et al., 2011). The maximum possible loading of BC on each filter (L_{maxBC}, g cm^{-2}) for a given T_{tot} is calculated by assuming that all the absorption from $\lambda = 650$–700 nm is due to BC ($f_{BC\_650-700} = 1$) and calibrating the attenuation of transmitted light through the sample filter from $\lambda = 650$–700 nm against a calibration curve created with commercially produced BC as described in Grenfell et al. (2011).

The best estimate of the BC loading on each filter, L_{BC} (g cm^{-2}), is determined by

$$L_{BC} = L_{maxBC} \cdot f_{BC\_650-700}. \quad (3)$$

The best estimate of BC concentration on a filter, C_{BC} (gC g^{-1}), is calculated by multiplying L_{BC} by the exposed area of the filter, A (cm^2), and dividing by the mass of meltwater filtered, M (g), as shown in Eq. (4):

$$C_{BC} = L_{BC} \cdot \frac{A}{M}. \quad (4)$$

The maximum concentration of BC on a filter, assuming BC is responsible for the total absorption in the 650–700 nm λ interval (C_{maxBC}), is calculated as shown in Eq. (5):

$$C_{maxBC} = L_{maxBC} \cdot \frac{A}{M}. \quad (5)$$

The total measured absorption optical depth (T_{tot}) of each filter can be represented as the sum of the optical depth associated with BC material (T_{BC}) and the optical depth associated with nonBC material (T_{nonBC}) on each filter.

$$T_{tot}(\lambda) = T_{BC}(\lambda) + T_{nonBC}(\lambda) \quad (6)$$

T_{tot} is measured directly by the spectrophotometer. T_{BC} is calculated by multiplying L_{BC} by the mean average mass absorption efficiency of BC ($\beta_{BC} \sim 48\,000$ m^2 g$_{BC}^{-1}$ at $\lambda = 675$ nm), which is determined from Mie scattering calculations (R. Brandt, personal communication, 2010). We calculate T_{nonBC} at various wavelengths using Eq. (7):

$$T_{nonBC}(\lambda) = T_{nonBC}(\lambda = 675 \text{ nm}) \cdot \left(\frac{\lambda(\text{nm})}{675}\right)^{-Å_{nonBC}}. \quad (7)$$

Here, we assume $Å_{BC} = 1$ and $Å_{nonBC} = 5$ in the wavelength range $\lambda = 298$–412 nm to calculate the optical properties of

BC and nonBC (including T_{BC} and T_{nonBC}) over that λ range. We use the optical properties of BC and nonBC to calculate the actinic flux profile in the snow at South Pole, Summit, and Dome C. We discuss the sensitivity of assuming $Å_{nonBC} = 5$ in Sect. 3.6.

2.2 Inherent optical properties of BC, nonBC, and snow

In addition to the concentration of light-absorbing impurities or the amount of absorption due to impurities in the snowpack, the inherent optical properties (IOPs) of the snowpack must also be known or estimated in order to calculate snowpack actinic flux. Inherent optical properties (IOPs), such as extinction coefficients (Kext) and co-albedos of single scattering ($c\varpi$), describe the absorption, scattering, and extinction properties of a material (e.g., ice grains, BC, HULIS). Kext (cm^{-1}) describes the amount of radiation removed from a beam of radiation traveling through a volume with a given cross-sectional area and length. $c\varpi$ (dimensionless, e.g., cm cm^{-1}) describes the amount of absorption compared to extinction (scattering + absorption) in a medium. IOPs vary with λ for most materials. The effective IOPs for a given λ needed for a snowpack containing contaminants can be written

$$Kext_{tot} = \sum_i Kext_i \quad \text{and} \quad (8)$$

$$c\varpi_{eff} = \frac{\sum_i c\varpi_i \cdot Kext_i}{Kext_{tot}}, \quad (9)$$

where $Kext_{tot}$ is the total extinction coefficient in the impurity-laden snowpack and $Kext_i$ represent the individual extinction coefficients for ice and impurities. Here, i indicates the components of the snowpack: ice and impurities (BC and nonBC). $c\varpi_{eff}$ is the effective co-albedo of single scattering (1 single scattering albedo) of the impurity-laden snowpack, and $c\varpi_i$ represents the individual co-albedos of single scattering for ice and impurities in the snow. The extinction coefficients and co-albedos of single scattering for snow, BC, and nonBC used in Eqs. (8) and (9) are given below.

The extinction coefficient for snow ($Kext_{snow}$) can be expressed as (Wiscombe and Warren, 1980)

$$Kext_{snow} = \frac{3 Q_{ext} \cdot \rho_{snow}}{4 r_e \cdot \rho_{ice}}, \quad (10)$$

where Q_{ext} is the extinction efficiency for snow grains (dimensionless, 2.01 at 305 nm), ρ_{snow} is snow density (g cm^{-3}), ρ_{ice} is the density of ice (0.917 g cm^{-3}), and r_e is the radiation equivalent mean grain radius (cm) (Hansen and Travis, 1974). r_e is inversely proportional to specific surface area (SSA), where SSA $= 3/(r_e \cdot \rho_{ice})$.

Table 2. The correction factor (Corr(μ_o)) used in Eq. (13) and Eq. (15), where $\mu_o = $ cosine of the solar zenith angle (θ).

θ	10°	20°	30°	40°	50°	60°	70°	80°	85°
μ_o	0.985	0.940	0.866	0.766	0.643	0.500	0.342	0.174	0.087
Corr(μ_o)	1.061	1.063	1.063	1.063	1.058	1.047	1.023	0.973	6.993

The extinction coefficient for BC (Kext$_{BC}$) in the snow can be calculated using the following equation:

$$\text{Kext}_{BC} = \frac{\beta_{BC} \cdot C_{BC} \cdot \rho_{snow}}{c\varpi_{BC}}, \tag{11}$$

where $c\varpi_{BC}$ is the single scattering co-albedo for BC (0.61 at 305 nm (R. Brandt, personal communication, 2010)). The wavelength dependence of the IOPs for both snow grains and soot particles are determined from Mie theory.

The extinction coefficient of nonBC material (Kext$_{nonBC}$) is calculated using

$$\text{Kext}_{nonBC} = \frac{T_{nonBC} \cdot \left(\frac{A}{M}\right) \cdot \rho_{snow}}{c\varpi_{nonBC}}, \tag{12}$$

where $c\varpi_{nonBC}$ is the co-albedo of single scattering for nonBC material. The contribution of scattering by BC and nonBC is insignificant because Kext$_{tot}$ is dominated by snow grain scattering (see denominator of Eq. (9)). Also, the co-albedos of single scattering cancel in the numerator of Eq. (9), leaving only the terms associated with the absorption of BC, nonBC, and snow grains. Therefore any value of $c\varpi_{nonBC}$ (between 0 and 1) can be used in the parameterization (here, we use $c\varpi_{nonBC} = 1$). In Eq. (12), if additional absorbers are to be included, the attenuation coefficient can be easily developed from a direct extension of Eqs. (8) and (9) and appropriate modifications to equations of the form of Eq. (11).

2.3 Snowpack actinic flux parameterization

Once the IOPs are calculated for snow grains and impurities and combined to determine the effective IOPs of the snowpack at various λ, the effective IOPs are used to calculate vertical profiles of the actinic flux. The snowpack radiative transfer model used here is a 4-stream plane parallel radiative transfer model that uses the discrete ordinates method (DOM) with a δ-M transformation as described in Grenfell (1991). The 4-stream approximation provides better than 1 % numerical accuracy in albedo and absorptivity relative to exact high-order models for optical properties representative of snow (Wiscombe, 1977), and produces results identical to those from the DISORT model (Stamnes et al., 1988). We use this snowpack radiative transfer model (Grenfell, 1991) to develop a parameterization to calculate the depth-dependent actinic flux profile in snowpacks. The motivation to develop this parameterization is based on the need to include snowpack chemical processes in large-scale models of the atmosphere in order to estimate the impact of these processes on

regional-scale nitrogen and oxidant budgets. This parameterization is based on the δ-Eddington formulation (Wiscombe and Warren, 1980) modified by a correction factor from the 4-stream DOM model (Grenfell, 1991), and accounts for the spatio-temporal variations in the properties of the snowpack and ambient lighting conditions. New values of the optical properties of ice (Warren and Brandt, 2008) have been incorporated, which indicate much greater UV transmission in the snowpack than in previous work (Wolff et al., 2002). We vary r_e with depth in the modeled snowpack following observed vertical r_e profiles in snow pits near Dome C station (Gallet et al., 2011), but the vertical r_e profiles and snow density in this parameterization can easily be altered in order to calculate actinic flux profiles in a wide range of snow types. These equations retain the general capability to vary the properties of the snow to represent actinic flux accurately over a wide range of snow conditions present in Antarctica and Greenland, provided that the snow cover is deeper than three times z_e ($3z_e$). By this depth, 95 % of radiation in snow has been attenuated. This parameterization is straightforward to implement into large-scale models of the atmosphere using calculated or assumed values of C_{BC}, f_{nonBC}, r_e and ρ_{snow}.

For collimated incident radiation at the surface ($z = 0$),

$$\left[\frac{I_o(\lambda, z = 0)}{F_{inc}(\lambda)}\right]_{direct} = \left[\frac{0.577 + \mu_o}{0.577 \cdot \mu_o}\right] \cdot \text{Corr}(\mu_o), \tag{13}$$

where $I_o(\lambda, z = 0)_{direct}$ is the snowpack actinic flux from direct beam radiation at the surface, $F_{inc}(\lambda)_{direct}$ (photons cm^{-2} s^{-1} nm^{-1}) is the direct downwelling irradiance at the surface which has been integrated over wavelength, μ_o is the cosine of the solar zenith angle (θ), and Corr(μ_o) is a correction factor for θ (see Table 2). The magnitude of the correction factor is less than 6.4 % for all θ less than 85°. For $\theta > 85°$, the correction factors are greater than 6.4 % because these θ are not well represented by the δ-Eddington approximation. However, solar radiation levels are very low at these θ, so the large correction factors have little influence on the parameterization.

Because the snowpack is such a strong volume scatterer in the UV (single scattering albedo > 0.9999), the direct beam downwelling irradiance, if present, becomes negligible within 2 cm of the upper surface of a thick snowpack. Thus it is convenient to define a reference depth (z_{ref}) of 2 cm below which the radiation field is purely diffuse.

For $z \geq z_{ref}$, $I_o(\lambda, z)_{direct}$ for collimated incident radiation follows an exponential decay law that depends on the physical properties of the snowpack and the concentration of

impurities such as BC and nonBC as follows:

$$\left[\frac{I_o(\lambda, z \geq z_{ref})}{F_{inc}(\lambda)}\right]_{direct} = G(z_{ref}, \mu_o) \cdot e^{-0.60 \cdot \Upsilon \cdot (z - z_{ref})}, \quad (14)$$

where G is a factor designed to treat the non-exponential decay of radiation in the top 2 cm. G is calculated in Eq. (15):

$$G(z_{ref}, \mu_o) = 3(0.577 + \mu_o) \cdot e^{-0.60 \cdot \Upsilon \cdot z_{ref}} \text{Corr}(\mu_o), \quad (15)$$

and the attenuation coefficient for diffuse radiation, Υ, (cm^{-1}) is expressed as

$$\Upsilon = (c\varpi_{eff})^{\frac{1}{2}} \cdot \text{Kext}_{tot} = \text{Kext}_{tot}^{\frac{1}{2}} \cdot \left[\sum_i c\varpi_i \cdot \text{Kext}_i\right]^{\frac{1}{2}}. \quad (16)$$

For the diffuse component of the actinic flux, $I_o(\lambda, z)_{diffuse}$ follows an exponential decay law beginning from the snow surface ($z = 0$):

$$\left[\frac{I_o(\lambda, z)}{F_{inc}(\lambda)}\right]_{diffuse} = 3.831 \cdot e^{-0.60 \cdot \Upsilon \cdot z}, \quad (17)$$

where $F_{inc}(\lambda)_{diffuse}$ (photons $cm^{-2} s^{-1} nm^{-1}$) is the diffuse downwelling irradiance at the surface, which has been integrated over wavelength. Because of strong Rayleigh scattering in the UV, there is a significant diffuse component to the incident radiation even for cloud free cases.

When both the direct and diffuse components of the downwelling irradiance are present, the combined (direct + diffuse) actinic flux, $I_o(\lambda, z)$ (photons $cm^{-2} s^{-1} nm^{-1}$) at a given depth (z) and wavelength (λ) is calculated as

$$I_o(\lambda, z) = \left\{\left[\frac{I_o(\lambda, z)}{F_{inc}(\lambda)}\right]_{diffuse} \cdot (f_{dif}) + \left[\frac{I_o(\lambda, z)}{F_{inc}(\lambda)}\right]_{direct} \cdot (1 - f_{dif})\right\}$$
$$\cdot [F_{inc}(\lambda)]_{tot}, \quad (18)$$

where f_{dif} is the fraction of diffuse incident radiation compared to total (direct + diffuse) radiation and $F_{inc}(\lambda)_{tot}$ (photons $cm^{-2} s^{-1} nm^{-1}$) is the sum of the direct ($F_{inc}(\lambda)_{direct}$) and diffuse ($F_{inc}(\lambda)_{diffuse}$) downwelling irradiance at the surface. Equation (18) can be integrated over depth and wavelength to calculate the total actinic flux ($\text{II}_o(\Delta\lambda_j, \Delta z_i)$) (photons cm s^{-1}) contributing to photochemical reactions (see Appendix A).

We use the Fast-J radiative transfer program (Wild et al., 2000) in the GEOS-Chem global chemical transport model (www.geos-chem.org) (Bey et al., 2001) to calculate the diffuse and direct downwelling solar radiation at the surface at different locations in Greenland and Antarctica in seven wavelength bins between $\lambda = 289$ nm and $\lambda = 850$ nm. We specify a UV surface albedo of 0.996 in GEOS-Chem based on discrete ordinate method results (Grenfell, 1991). The above parameterization (Eq. 18) is used to examine how each variable (e.g., BC, nonBC, r_e, θ) influences the actinic flux ($\lambda = 305$ nm) profile in the snowpack.

2.4 Calculating the depth dependent lifetime of NO_x in snowpack

The majority of NO_x associated with nitrate photolysis is produced above $3z_e$, since most of the radiation in snow has been attenuated above that depth. Due to our calculated $3z_e > 1.5$ m in some locations (Sect. 3.3), we examine whether the NO_x produced via NO_3^- photolysis at depth will escape into the overlying atmosphere via wind pumping before being re-oxidized to HNO_3 within the snowpack interstitial air. Although the diffusion of NO_x from the snowpack interstitial air to the overlying atmosphere will also play a role in its transport, we exclude diffusion within the snowpack interstitial air from our analysis for reasons discussed in Sect. 3.5. We define the wind pumping lifetime ($\tau_{wind\ pumping}$) as the lifetime of NO_x in the snowpack interstitial air against transport to the overlying atmosphere via wind pumping. The chemical lifetime ($\tau_{chemical}$) represents the lifetime of NO_x in the snowpack interstitial air against conversion to HNO_3, $BrONO_2$, and $IONO_2$ in the snowpack via the following reactions:

$$NO_2 + OH \rightarrow HNO_3, \quad (R1)$$
$$NO_2 + BrO \rightarrow BrONO_2, \quad \text{and} \quad (R2)$$
$$NO_2 + IO \rightarrow IONO_2. \quad (R3)$$

The characteristic escape time of NO_x (and other gaseous compounds in the snowpack) for wind pumping is calculated according to Waddington et al. (1996):

$$\tau_{wind\ pumping} = \frac{1}{C} \cdot \frac{\lambda_s}{h} \cdot \left[\frac{\mu/\rho_{air}}{U\lambda_s}\right] \cdot \frac{\Omega\lambda_s^2}{2\pi K} \cdot \frac{\lambda_s}{U} \cdot e^{\frac{2\pi z}{\lambda_s}}, \quad (19)$$

where, λ_s is sastrugi wavelength (cm), h is sastrugi height (cm), U is horizontal wind speed at the surface (cm s^{-1}) (see Table 3), Ω is porosity (0.673), ρ_{air} is air density (g cm^{-3}) calculated from the ideal gas law and the hypsometric equation using average summer air temperatures and the altitude of each station, μ is air viscosity (1.6×10^{-4} g cm^{-1} s^{-2}), K is snow permeability (8×10^{-6} cm^2), and C is a constant of proportionality ($\sim$3) (Waddington et al., 1996).

The lifetime of NO_x in snowpack interstitial air against conversion to HNO_3, $BrONO_2$, and $IONO_2$ is calculated according to Seinfeld and Pandis (1998):

$$\tau_{NO_2+X} = (k_X[X])^{-1} \cdot \left(1 + \frac{[NO]}{[NO_2]}\right), \quad (20)$$

where X = OH, BrO, or IO, and k_X is the corresponding rate constant (cm^3 molec^{-1} s^{-1}) for Reactions (R1)–(R3) from Sander et al. (2006).

The effective lifetime of NO_x against chemical conversion is calculated as

$$\tau_{chemical} = \left(\frac{1}{\tau_{NO_2+OH}} + \frac{1}{\tau_{NO_2+BrO}} + \frac{1}{\tau_{NO_2+IO}}\right)^{-1}. \quad (21)$$

Table 3. Values for the variables used to calculate the lifetime of NO$_x$ in the snowpack interstitial air against escape to the overlying atmosphere via wind pumping during austral summer at Dome C and South Pole and during summer at Summit. The base-case values are provided along with the full range of values used in the sensitivity studies in parentheses.

	Dome C	Summit	South Pole	References
Sastrugi height (h, cm)	5.5 (3–8)	5 (3–8)	19.5 (9–25)	Albert and Hawley (2002); Six and Warren, unpublished data; Warren et al. (1998)
Sastrugi, wavelength, (λ, cm)	55 (30–80)*	135 (50–225)	170 (70–400)	Albert and Hawley (2002); Six and Warren, unpublished data; Warren et al. (1998)
Wind speed (U, cm s^{-1})**	280 (150–500)	430 (200–600)	470 (420–520)	Albert and Hawley (2002); Aristidi et al. (2005); Orvig (1970)
Permeability (K, cm^2)	8 × 10^{-6} (8 × 10^{-5}-8 × 10^{-7})			Waddington et al. (1996)
Viscosity (μ, g cm^{-1} s^{-2})	1.6 × 10^{-4}(1 × 10^{-3}-1 × 10^{-6})			Waddington et al. (1996)
Snow density (ρ, g cm^{-3})	0.36 (0.1–0.9)			Albert and Shultz (2002); Gallet et al. (2011); Grenfell et al. (1994)
Tortuosity (ξ, cm cm^{-1})	1.33 (0.5–4)			Pinzer et al. (2010)

* Sastrugi aspect ratio (height/width) of 0.1 using h from unpublished results from Six and Warren (2006) to calculate λ at Dome C.
** Wind speeds at South Pole from Orvig (1970) are 10 m wind speeds. 10 m wind speeds should be used in Eq. (19) to calculate $\tau_{\text{wind pumping}}$ when available.

Formation of HNO$_3$(g) is considered a sink for snowpack NO$_x$ because the lifetime of HNO$_3$(g) against photolysis (10–30 days in the tropics and longer in polar regions (Jacob et al., 1996; Tie et al., 2001)) is much longer than its lifetime against deposition to the surface in polar regions (3.5–10 h) (Slusher et al., 2002; Wang et al., 2007). Hydrolysis of BrONO$_2$ and IONO$_2$ on the surface of snow crystals to form HNO$_3$ and HOBr/HOI is also considered a sink for snowpack NO$_x$. However, BrONO$_2$ and IONO$_2$ can also photolyze to Br + NO$_3$ and I + NO$_3$, respectively (or less commonly, BrO + NO$_2$ and IO + NO$_2$, respectively).

The lifetime of BrONO$_2$ with respect to photolysis is calculated as

$$\tau_{\text{BrONO}_2\_\text{photolysis}} = J_{\text{BrONO}_2}^{-1}$$
$$= (\text{II}_\text{o}(\Delta\lambda_j, \Delta z_i) \cdot \phi_{\text{BrONO}_2} \cdot \sigma_{\text{BrONO}_2})^{-1}, \tag{22}$$

where $\text{II}_\text{o}(\Delta\lambda_j, \Delta z_i)$ is the total actinic flux in the $\lambda = 289$–500 nm bin at a specified depth in the snowpack, ϕ_{BrONO_2} is the quantum yield for the photolysis of BrONO$_2$ (0.15 for $\lambda > 300$ nm) (Sander et al., 2006), and σ_{BrONO_2} is the absorption cross section for BrONO$_2$ (Sander et al., 2006).

To calculate depth-dependent $\tau_{\text{BrONO}_2\_\text{photolysis}}$ in the snowpack, we use our calculated values of $\text{II}_\text{o}(\Delta\lambda_j, \Delta z_i)$ at $\lambda = 289$–500 nm (wavelengths relevant to BrONO$_2$ photolysis) (Burkholder et al., 1995) from Eq. (18) using $\mu_o = 60°$and $r_\text{e} = 100$ µm at local solar noon in January at Dome C and South Pole and in June at Summit. To estimate F$_{\text{inc}}$ at $\lambda < 500$ nm in the $\lambda = 412$–850 nm range (con-

sistent with Fast-J), we multiply the amount of direct radiation in the $\lambda = 412$–850 nm wavelength bin by the fraction [(500–412 nm)/(850–412 nm)]. This simplification is appropriate given that the solar flux is relatively constant throughout the $\lambda = 412$–850 nm range. The mean σ_{BrONO_2} in each wavelength bin is calculated by taking the average σ_{BrONO_2} within each bin from Burkholder et al. (1995). The photolysis rates are summed over the bins to create a depth-dependent BrONO$_2$ photolysis rate from $\lambda = 289$–500 nm.

The lifetime of BrONO$_2$ with respect to hydrolysis is calculated as

$$\tau_{\text{BrONO}_2\_\text{hydrolysis}} = (k_{\text{BrONO}_2+\text{H}_2\text{O(s)}})^{-1}, \tag{23}$$

where

$$k_{\text{BrONO}_2+\text{H}_2\text{O(s)}} = \left(\frac{r_\text{e}}{D_\text{g}} + \frac{4}{\upsilon\gamma}\right)^{-1} \cdot \text{SA}. \tag{24}$$
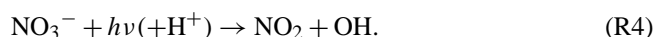
Here, $k_{\text{BrONO}_2+\text{H}_2\text{O(s)}}$ is the first-order rate constant for uptake of BrONO$_2$ on the ice crystal surface (molec cm^{-3} s^{-1}), r_e is the snow grain radius (0.01 cm), D_g is the gas-phase molecular diffusion coefficient of BrONO$_2$ in air (0.2 cm^2 s^{-1}), γ is the reaction probability (0.2) (Sander et al., 2006), υ is the mean molecular speed of BrONO$_2$ in the gas phase (3 × 10^4 cm s^{-1}), and SA is the corresponding snow grain surface area per unit volume of air (177 cm^2 cm^{-3}) calculated in Eq. (25):

$$\text{SA} = \frac{3 \cdot \rho_{\text{snow}}}{r_\text{e} \cdot (\rho_{\text{ice}} - \rho_{\text{snow}})}. \tag{25}$$

Table 4 contains the values for the variables used to calculate τ_{chemical} (Eq. 21). Although the formation of IONO$_2$ may influence τ_{chemical}, IO in polar regions has only been measured at the coast (Saiz-Lopez et al., 2008), so we assume [IO] = 0 at South Pole, Dome C, and Summit (and evaluate this assumption in Sect. 3.4). We use OH, BrO, NO, and NO$_2$ vertical snowpack concentration profiles at Summit from Thomas et al. (2011), which include the effect of transport in the snow interstitial air. The vertical chemical profiles from Thomas et al. (2011) at Summit indicate firn air NO$_x$ concentrations on the order of 10^{-9} mol mol^{-1}, which is in good agreement with measured firn air NO$_x$ concentrations at Dome C (Frey et al., 2013). We examine the sensitivity of the lifetime of NO$_x$ with respect to chemical sinks using a range of summertime concentrations for each species at each location (see Table 4 for concentration ranges).

2.5 NO$_x$ flux calculations

Nitrate photolysis in the snowpack is represented as (Warneck and Wurzinger, 1988)

$$NO_3{}^- + h\nu (+H^+) \rightarrow NO_2 + OH. \tag{R4}$$

The total potential flux of NO$_x$ out of the snowpack from the photolysis of nitrate, F_{NO_x} (molec cm^{-2} s^{-1}), is calculated via

$$F_{\text{NO}_x} = \sigma_{\text{NO}_3^-}(\lambda) \cdot \phi_{\text{NO}_x}(T, \text{pH}) \cdot \text{II}_o(\Delta\lambda_j, \Delta z_i) \cdot [\text{NO}_3{}^-]. \tag{26}$$

In Eq. (26), $\sigma_{\text{NO}_3^-}$ is the absorption cross section for nitrate photolysis (cm^2), ϕ_{NO_x} is the quantum yield for nitrate photolysis (unitless), $\text{II}_o(\Delta\lambda_j, \Delta z_i)$ is the depth-integrated total actinic flux from $z = 0$ to $3z_e$ in a given wavelength bin (photons cm s^{-1}), and [NO$_3^-$] is the average nitrate concentration over the integration depth (molec cm^{-3}). Please see the Appendix A for calculation of $\text{II}_o(\Delta\lambda_j, \Delta z_i)$.

F_{NO_x} is calculated for local solar noon conditions in January at Dome C and South Pole and in June at Summit using $\text{II}_o(\Delta\lambda_j, \Delta z_i)$ calculated from Eq. (18) in the $\lambda = 298$–345 nm range and mean $\sigma_{\text{NO}_3^-}$ and ϕ_{NO_x} from Sander et al. (2006). The wavelength range from 298–345 nm encompasses four λ bins from the Fast-J program: 298–307, 307–312, 312–320, and 320–345 nm. We use the mean absorption cross sections in each λ bin. We use the average daily mean January temperatures at Dome C (243 K) (Frey et al., 2009) and South Pole (244 K) (Orvig, 1970) and June temperatures at Summit (257 K) (Steffen and Box, 2001) to calculate the temperature dependent quantum yield for NO$_x$ (ϕ_{NO_x}) from Chu and Anastasio (2003). The monthly mean overhead ozone column abundance in GEOS-Chem for January is 293 DU at South Pole and 306 DU at Dome C, and for June is 349 DU at Summit.

We choose a range of nitrate concentrations appropriate for polar snowpacks based upon observations in the top 1 m of snowpack at each location (Dibb et al., 2004, 2007, 2010;

Frey et al., 2009). The upper 2 cm of snowpack in polar regions have considerably higher nitrate concentrations compared to depths below 2 cm in the snowpack and experience a sharp decay in concentration from the surface to 2 cm (Frey et al., 2009; Rothlisberger et al., 2000). Below 2 cm, [NO$_3^-$] decreases more gradually until concentrations oscillate (representing seasonality) around a relatively constant value. In this study, we calculate the flux of NO$_x$ from the snowpack (F_{NO_x}) using a two layer approach ($z = 0 - z_{\text{ref}}$ and $z = z_{\text{ref}} - 3z_e$) and assume a constant snowpack [NO$_3^-$] below 2 cm.

It is thought that only nitrate in the surface layer of ice crystals is photolyzable, (Boxe et al., 2005; Boxe and Saiz-Lopez, 2008; Chu and Anastasio, 2003; Dubowski et al., 2001) while nitrate in the ice lattice does not contribute. Since the fraction of total nitrate in the surface layer is unknown, we assume that all nitrate in the snow is available for photolysis and that all NO$_x$ produced in the surface layer is transferred to the adjacent interstitial air. This combined with the fact that we assume that all NO$_x$ produced in the snowpack from the photolysis of nitrate escapes to the overlying atmosphere suggests that our calculations provide an upper limit for the flux of NO$_x$ from the snow.

3 Results and discussion

3.1 BC and nonBC impurity concentrations from the filtering of snow samples

Table 1 describes the location and depth, the best estimate of the concentration of BC on the filter (C_{BC}), the Ångström exponent (Å) measured in the 450–600 nm λ range, and the estimated fraction of absorption in the $\lambda = 650$–700 nm and $\lambda = 298$–345 nm ranges due to nonBC impurities ($f_{\text{nonBC\_650-700}}$, $f_{\text{nonBC\_298-345}}$) for snow samples averaged by location. Appendix B contains similar information about each individual snow sample.

In the snow samples collected near (< 0.5 km) and away (11 km) from the Dome C station, the average C_{BC} is 2.1 ± 1.3 ng g^{-1} and 0.6 ± 0.2 ng g^{-1}, respectively. In the snow samples collected 20–40 km from the Summit station, the average C_{BC} is 1.4 ± 0.3 ng g^{-1}. C_{BC} in snowpack near the station at Dome C is 1.5–3.5 times greater than C_{BC} in snowpacks away from the stations at Dome C and Summit, highlighting the influence of station activity on impurity levels in the local snowpack. Hagler et al. (2008) present similar results for Summit, Greenland. C_{BC} in Greenland snow is over two times higher than C_{BC} in snow 11 km away from Dome C station. This combined with the low accumulation rate at Dome C (3 g cm^{-2} yr^{-1}) (Rothlisberger et al., 2000) compared to Summit (25 g cm^{-2} yr^{-1}) (Dibb and Fahnestock, 2004) highlights the higher concentration of pollutants in the Northern Hemisphere compared to the Southern Hemisphere.

Table 4. Chemical concentrations (pptv) used in the NO_x chemical lifetime ($\tau_{chemical}$) equations. The summertime base-case values of boundary layer $[NO_2]$, $[NO]$, $[OH]$, and $[BrO]$ are provided along with the range of values used in the sensitivity studies in parentheses.

	Dome C	South Pole	Summit	References
$[NO_2]$	102 (14–190)	175 (0–350)	15 (0–30)	Davis et al. (2004); Frey et al. (2013); Thomas et al. (2011)
$[NO]$	111 (22–200)	136 (0–550)	25 (0–50)	Davis et al. (2004); Frey et al. (2013); Thomas et al. (2011)
$[OH]$	0.08 (.033–.13)*	0.08 (.033–.13)	0.22 (.14–.28)	Mauldin et al. (2010); Sjostedt et al. (2007)
$[BrO]$	0.5 (0.25–1)**	0.5 (0.25–1)**	2 (0–4)	Stutz et al. (2011); Yang et al. (2005)

* South Pole [OH] measurements from Mauldin et al. (2010) used at Dome C.
** Modeled [BrO] concentrations from Yang et al. (2005) used at Dome C and South Pole.

Measured Ångström exponents for the particulate material on the filters fall between the values of Å $= 1$, considered representative of pure BC, and Å $= 5$ for HULIS (Doherty et al., 2010), and are smaller than Å~ 3.8 for dust (Zender et al., 2003). This suggests a mixture of nonBC and BC impurities in both the snowpacks near and remote from the station. The similarity in the Ångström exponents at remote locations near Summit and Dome C suggests that the ratio of C_{BC} to C_{nonBC} and the type of nonBC material is similar in Greenland and Antarctica, even with the factor of 2 difference in C_{BC} at Summit and Dome C.

In all snow samples, nonBC material is responsible for 20–29 % of the absorption at $\lambda = 650\text{-}700$ nm and 86–89 % of absorption at $\lambda = 298\text{–}345$ nm (photochemically relevant region). The increase in nonBC absorption in the UV results from assuming an Ångstrom exponent of nonBC material of 5. At $\lambda = 650\text{–}700$ nm, BC is the dominant absorber in the snow, but at $\lambda = 298\text{–}345$ nm nonBC material dominates absorption. The fraction of nonBC absorption (f_{nonBC}) increases and the concentration of BC (C_{BC}) decreases with increasing distance from the station. The mean change in the fraction of absorption by BC or nonBC from $\lambda = 298\text{–}345$ nm between snow near and 11 km away from Dome C station is 3.4 %, while the corresponding change in BC concentration is 71.4 %. While we cannot quantify the concentration of nonBC (C_{nonBC}), we can infer that the station is a source of both BC and nonBC because the change in the f_{nonBC} is smaller than the change in C_{BC}. This suggests that both BC and nonBC concentrations are decreasing away from the station (since f_{nonBC} changes less drastically than C_{BC}), but that C_{BC} is decreasing at a faster rate compared to C_{nonBC}.

3.2 Sensitivity of snowpack actinic flux to variations in atmospheric conditions and snowpack radiative properties

Figure 2 compares the vertical actinic flux profile in the snowpack calculated according to Eq. (18) to the profile calculated using the full snowpack radiative transfer model (Grenfell, 1991) for a deep (depth > 3 m) snowpack. For this comparison, we use typical remote Antarctic conditions at $\lambda = 305$ nm: $r_e = 100$ µm, $\rho_{snow} = 0.36$ g cm^{-3}, and $C_{BC} = 0.3$ ng g^{-1}. We assume $C_{nonBC} = 0$ ng g^{-1} for simplic-
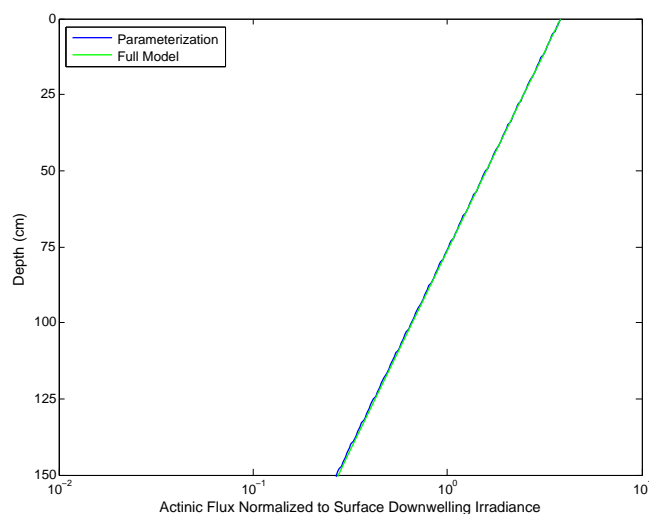

Fig. 2. Actinic flux profile normalized to surface downwelling radiation determined by our parameterization (Eq. 18) and the full model (Grenfell, 1991) for a representative deep (depth > 3 m) snowpack. For this comparison, the incident radiation field is entirely diffuse, $\lambda = 305$ nm, $\theta = 60°$, $r_e = 100$ µm, $C_{BC} = 0.3$ ng g^{-1}, and $C_{nonBC} = 0$ ng g^{-1}. For an isotropic radiation field, the ratio of actinic flux to surface downwelling radiation is equal to 4. This ratio is somewhat less than 4 for the present cases depending on the solar zenith angle and amount of cloud cover.

ity and assume a constant reference density with depth of 0.36 g cm^{-3}. The parameterization shows good agreement (within 2 % in the top 150 cm and within 8 % from 150–500 cm) with the full snowpack radiative transfer model for the above scenario and additional scenarios using various combinations of snowpack and radiative properties (not shown).

Figure 3 illustrates the dependence of snowpack actinic flux on wavelength (λ), impurity concentration (C_{BC} and f_{nonBC}), snow grain effective radius (r_e) (Hansen and Travis, 1974), and solar zenith angle (θ). Snow density (ρ_{snow}) was also varied around a typical range, but the results are not shown in Fig. 3 because changes in ρ_{snow} do not influence the actinic flux profile significantly. For all of the normalized actinic flux profiles in Fig. 3, 89 % of the absorption at $\lambda = 305$ nm is due to nonBC material. Figure 3a shows
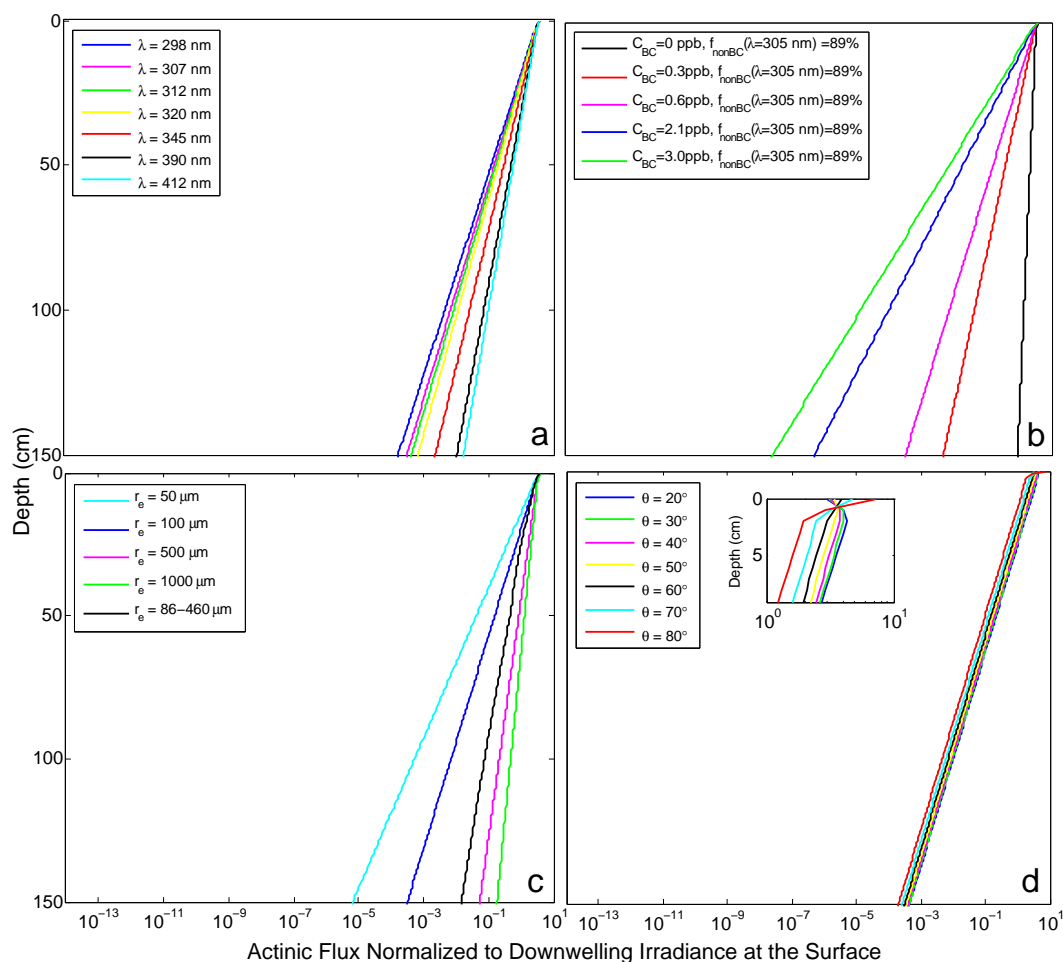
Fig. 3. Dependence of the actinic flux depth profile on wavelength, λ **(a)**, concentration of black carbon in the snowpack, C_{BC} **(b)**, ice grain radius, r_e **(c)**, and solar zenith angle, θ **(d)**. In **(c)**, the black line is the depth profile of actinic flux using vertical r_e profile ranging from 86 µm at the snow surface to 460 µm at a depth of 500 cm. In **(d)**, a zoomed in view of the top 10 cm is provided. In **(a–d)**, Å = 2.90, $f_{nonBC\_305} = 89$ %, and λ, C_{BC}, r_e, and θ were varied around a reference case of $\theta = 60°$, $r_e = 100$ µm, $\lambda = 305$ nm, $C_{BC} = 0.6$ ng g^{-1}.

that z_e decreases with decreasing λ. The λ dependence is primarily due to the fact that nonBC material is assumed to absorb radiation more effectively at shorter wavelengths (e.g., Å $\sim$5). If only BC is present, the λ dependence is negligible (not shown).

Figure 3b shows the strong dependence of z_e on BC and nonBC with the e-folding depth decreasing with increasing BC and nonBC absorption. As C_{BC} is increased, the concentration of nonBC is also increasing because of our assumption that $f_{nonBC} \approx 89$ % at $\lambda = 305$ nm. The range of C_{BC} in Fig. 3b (0.3–3 ng g^{-1}) represents the observed range of C_{BC} in Antarctica (Warren and Clarke, 1990; Warren et al., 2006). The snowpack actinic flux profile when $C_{BC} = 0$ is included for reference.

Figure 3c shows the strong dependence of z_e on radiation-equivalent ice grain radius (r_e) with z_e values decreasing with decreasing r_e (r_e is assumed constant with depth). The decrease of z_e with decreasing r_e is due to the increased scat-

tering that occurs as the number of grains per unit volume increases (see Eq. 10). The black curve in Fig. 3c is the snowpack actinic flux profile calculated when r_e is varied from 86 µm at $z = 0$ to 460 µm at $z = 500$ cm based on r_e measurements made near Dome C station by Gallet et al. (2011) that are linearly extrapolated below 50 cm. The average vertical r_e profile measured near Dome C station by Gallet et al. (2011) is applied to all snowpacks simulated in this study in absence of detailed vertical r_e profiles at South Pole and Summit, but we note that the vertical r_e profiles between these locations may vary. Sensitivity studies reveal that BC and nonBC impurities in the snow influence z_e more significantly than differences in r_e profiles, as long as the snowpacks are not experiencing melt.

Figure 3d shows the influence of the solar zenith angle (θ) on z_e for the case of collimated incident radiation. In the top 2 cm (inset of Fig. 3d), where direct radiation is scattered and converted to diffuse radiation, θ influences both the amount

Table 5. Calculated e-folding depths of actinic flux (z_e) in snow near the station and remote from the station in the designated clean-air sector for January at Dome C and South Pole and June at Summit for $\lambda = 305$ nm and $\lambda = 400$ nm. The range of e-folding depths represents the range between fully direct (smaller z_e) and fully diffuse (larger z_e) incident radiation conditions. Values of C_{BC}, f_{nonBC_305}, and f_{nonBC_400} used to calculate z_e at each location are shown.

| | | Wavelength (λ, nm) | | C_{BC} (ng g^{-1}) | f_{nonBC_305} (%) | f_{nonBC_400} (%) |
		305	400			
Dome C	Remote	18–22 cm	32–40 cm	0.6	89.8	77.2
	station	10–12 cm	18–21 cm	2.1	87.1	72.2
Summit	Remote	15–17 cm	23–28 cm	1.4	90.4	78.4
South Pole	Remote	26–31 cm	53–62 cm	0.3	89.8	77.2
	station	8–10 cm	15–18 cm	3.0	87.1	72.2

of radiation as well as the slope of the actinic flux profile in the snowpack. At $\theta < 50°$, the actinic flux increases with depth in the first 2 cm. This is because scattering by an individual snow particle is strongly in the forward direction, increasing the penetration of the photons; more scattering events are needed to deflect the photons that have entered the snowpack at small solar zenith angles back to the atmosphere (Bohren and Barkstrom, 1972). Below 2 cm, where the radiation is entirely diffuse, the slopes of the actinic flux profiles are the same for all values of θ. The depth profile for purely diffuse incident radiation is exponential and corresponds closely to the profile for $\theta = 54°$ under clear sky conditions.

The results shown in Fig. 3 suggest that for a given λ, and a plausible range of values for the variables considered (Table 3), impurity concentration (C_{BC} and C_{nonBC}) and radiation-equivalent mean ice grain radius (r_e) affect the actinic flux profile in snowpack most significantly. Due to the difficulty in measuring C_{nonBC} and its optical properties, the concentration and optical properties of nonBC material, such as HULIS, represent the largest uncertainty in calculations of snowpack actinic flux since nonBC material is responsible for over 85 % of absorption in the UV wavelengths relevant for photochemistry.

3.3 e-folding depth of actinic flux in the snowpack

Table 5 lists the z_e values for $\lambda = 305$ nm and $\lambda = 400$ nm for snow near the station at Dome C and South Pole and away from the station at Dome C, South Pole, and Summit calculated using Eq. (18) along with the observed C_{BC}, f_{nonBC_305}, and f_{nonBC_400} at each location. We also include observed C_{BC} in South Pole snowpack; $C_{BC} = 3$ ng g^{-1} was measured just downwind of the station and $C_{BC} = 0.3$ ng g^{-1} was measured in the clean air sector (close to and upwind of the Atmospheric Research Observatory) (Warren and Clarke, 1990). We assume f_{nonBC_305} and f_{nonBC_400} are similar at all wavelengths between South Pole and Dome C because both stations are located high on the Antarctic plateau, which allows us to quantify the influence

of nonBC material on UV/near-vis absorption at South Pole. In all cases, z_e is shallower at $\lambda = 305$ nm than at $\lambda = 400$ nm due to the wavelength dependence of the inherent optical properties of nonBC material (see Fig. 1). In snowpacks with low impurity concentrations (remote, polar snowpacks), z_e is even deeper because as r_e increases with depth, scattering decreases, thus decreasing the probability of radiation absorption by impurities. z_e values are a factor of 1.8–3.5 larger at remote locations (> 11 km) compared to locations near the stations (< 0.5 km) because C_{BC} and the absorption of nonBC material is 3.5–10 times greater in near-station snowpacks compared to remote snowpacks. The increase in absorption of nonBC material can be inferred because our observations suggest that the Ångström exponents are roughly similar between near-station and remote snowpacks. Our calculated z_e values compare well (within 30 %) with observed values, as detailed in Appendix C.

3.4 The depth-dependent lifetime of NO$_x$ in the snowpack

Figure 4 shows the chemical lifetime of NO$_x$ ($\tau_{chemical}$) in the snowpack against conversion to HNO$_3$ (τ_{NO_2+OH}) and BrONO$_2$ (τ_{NO_2+BrO}) for Summit. We assume that the formation of BrONO$_2$ represents a sink for NO$_x$ because the calculated lifetime of BrONO$_2$ against hydrolysis onto snow grains (0.0006 s) is much shorter than the lifetime against photolysis (3–5 min) due to the large surface area of snow grains in the snowpack (Michalowski et al., 2000). Thus, we consider Reactions (R1)–(R3) to be sinks for NO$_x$ in the snowpack. The vertical profiles of BrO, OH, NO, and NO$_2$ concentrations are determined using concentration profiles of OH, BrO, NO, and NO$_2$ from Thomas et al. (2011). At Summit, the chemical lifetime of NO$_x$ is mainly controlled by reactions with BrO when observed surface concentrations are scaled at depth to the actinic flux.

The chemical profiles of OH, BrO, and NO increase from the surface, reach a maximum in concentration at 5-10 cm depth, then decay exponentially, following the decay of actinic flux in the snowpack. Efficient transport to the

Table 6. Calculated and observed NO$_x$ fluxes (F_{NO_x}) near Dome C, Summit, and South Pole.

	Polar NO$_x$ fluxes (molec cm^{-2} s^{-1})*			
	Calculations (this work)		Observations	
Location	Remote	Station	Station	Reference
Dome C	4.4×10^8–1.7×10^9	3.2×10^8–1.2×10^9	6.9×10^8	Frey et al. (2013)
Summit	1.3–2.8×10^9		2.5×10^8	Honrath et al. (2002)
South Pole	7.7×10^8–2.2×10^9	3.3–9.8×10^8	3.8×10^{8}**	Oncley et al. (2004)

* NO$_x$ fluxes are calculated assuming that all NO$_x$ produced in the snowpack escapes to the atmosphere.
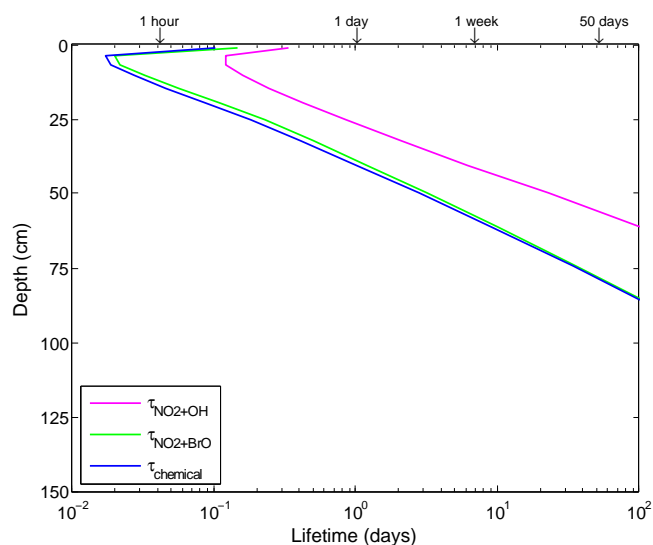** NO$_x$ flux estimated from a derived NO flux and photochemical equilibrium values of NO$_2$.

Fig. 4. Depth-dependent lifetime (days) of NO$_x$ in the snowpack against chemical conversion to HNO$_3$ (τ_{NO_2+OH}, pink curve), BrONO$_2$ (τ_{NO_2+BrO}, green curve), and the combination of the two reactions ($\tau_{chemical}$, blue curve) for near station snow at Summit. The lifetime curves are calculated using concentration profiles of BrO, OH, NO, and NO$_2$ from Thomas et al. (2011).

atmosphere above 5–10 cm depth combined with decreasing actinic flux with depth in the snowpack results in maximum OH, BrO, and NO concentrations at depths of 5–10 cm in the snowpack (Thomas et al., 2011). Model results from Thomas et al. (2011) show that NO$_2$ remains relatively constant with depth in the snowpack, likely because NO$_2$ has a longer lifetime than OH, BrO, and NO and its production rate and photolysis rate both decrease with depth.

Figure 5 shows the vertical profiles of $\tau_{chemical}$ and $\tau_{wind\ pumping}$ in remote snowpacks of Summit calculated using average summertime values of snow density, snow permeability, sastrugi wavelength, sastrugi height, wind speed, and boundary layer [OH], [BrO], [NO], and [NO$_2$] at Summit (Table 3). In Fig. 5, $\tau_{wind\ pumping}$ is shorter (more efficient) than $\tau_{chemical}$ at all depths, meaning that NO$_x$ efficiently escapes from the snowpack throughout most of the photochemically active zone. The full range of expected values

for each variable (snow density, snow permeability, sastrugi wavelength, sastrugi height, wind speed, [OH], [BrO], [NO], [NO$_2$]) in Eq. (19) ($\tau_{wind\ pumping}$) and Eq. (21) ($\tau_{chemical}$) are used in sensitivity studies. NO$_x$ efficiently escapes from the snowpack throughout most of the photochemically active zone when base-case conditions are considered and any value of snow density is assumed. $\tau_{chemical}$ is shorter than $\tau_{wind\ pumping}$, meaning that NO$_x$ in the photochemically active zone is more likely to convert to HNO$_3$ rather than escape to the atmosphere, for a permeability of 1×10^{-10} or less, a viscosity of 9×10^{-5} or greater, and a sastrugi aspect ratio (height/wavelength) greater than 0.16. If $\tau_{chemical}$ becomes shorter than $\tau_{wind\ pumping}$ at a depth closer to the snow surface than $3z_e$, the actinic flux should be integrated to a shallower depth than $3z_e$ when calculating the flux of NO$_x$ from the snowpack, F_{NO_x}, because a significant portion of NO$_x$ produced through photodenitrification would convert to HNO$_3$ before escaping to the atmosphere.

We have assumed [IO] = 0 in this study because IO that is produced in coastal regions due to biological activity quickly oxidizes and may deposit to coastal snow surfaces before being transported inland. However, if we assume IO concentrations are equal to the base-case BrO concentrations used in this study, our results are not changed. We find that the conversion of NO$_2$ to BrONO$_2$ and IONO$_2$ are equally dominant when concentrations of IO and BrO are equivalent due to similar reaction rate constants. The chemical concentrations of BrO, IO, and OH in the snowpack are highly uncertain, but are thought to be on the order of 10^{-12} mol mol^{-1} in the snowpack (Thomas et al., 2011). However, Frieß et al. (2010) observed IO concentrations at Neumayer on the order of 10^{-9} mol mol^{-1} while surface atmosphere observations were on the order of 10^{-12} mol mol^{-1}. If we use snowpack BrO and IO concentrations on the order of 10^{-9} mol mol^{-1}, we find that NO$_x$ is not efficiently ventilated to the atmosphere ($\tau_{chemical}$ is shorter than $\tau_{wind\ pumping}$ at all depths). In this scenario, a significant portion of the NO$_x$ produced through photodenitrification would convert to HNO$_3$ before escaping to the atmosphere at all depths.

Given the uncertainty in snowpack NO$_x$ profiles, we have not explicitly considered diffusion as a means to transport NO$_x$ from the snowpack interstitial air to the overlying
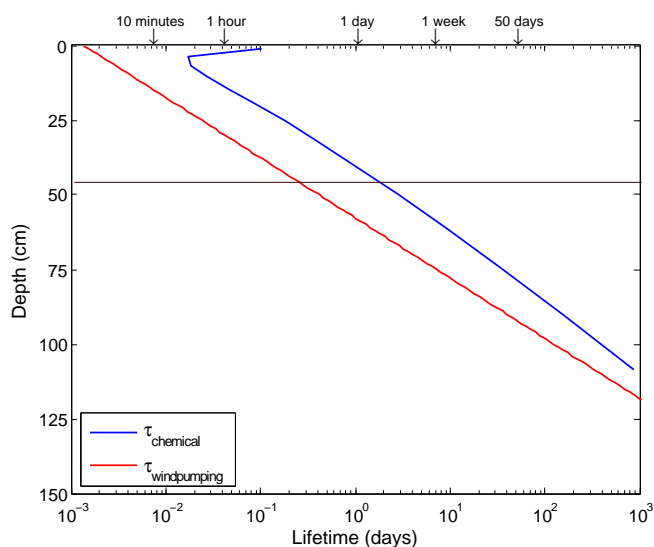
Fig. 5. Vertical profiles of $\tau_{\text{wind pumping}}$ (red) and τ_{chemical} (blue) in snow near the station at Summit. The profiles are calculated using typical Summit sastrugi and meterological information (Table 3) and Summit chemical profiles calculated in Thomas et al. (2011) (Fig. 4). The e-folding depth in near-station snow at Summit is not calculated in this study because C_{BC} and nonBC absorption are unknown. Three times the e-folding depth of actinic flux at $\lambda = 305$ nm ($3z_e$) for remote Summit snow is shown for reference (horizontal, black solid line), although $3z_e$ in near station snow is likely more shallow due to enhanced impurity concentrations from local station activities.

atmosphere, though diffusion is likely important in reality. The chemical profiles calculated in the Thomas et al. (2011) study suggest that the concentration of NO$_2$, NO, BrO, and OH are higher in the snow compared to the atmosphere until a depth of 20–30 cm. The profiles suggest that NO$_x$ produced by photodenitrification would diffuse towards the atmosphere from the snow surface to a depth of 20–30 cm, which is roughly 1–2 e-folding depths depending on snowpack impurity concentration. The inclusion of diffusion in our analysis would likely further shorten the lifetime of NO$_x$ against escape to the atmosphere. However, even without diffusion, wind pumping of NO$_x$ from the snowpack to the atmosphere is still dominant compared to NO$_x$ decay to HNO$_3$ when base-case conditions are assumed for variables used to calculate the wind pumping and chemical lifetime.

3.5 Results of NO$_x$ flux calculations

Table 6 shows the results of our calculated flux of NO$_x$ from the snowpack to the overlying atmosphere, F_{NO_x}, using observed nitrate concentrations as described in Sect. 2.5. To calculate the F_{NO_x}, we assume that the NO$_x$ lifetime against wind pumping is always shorter than the chemical lifetime of NO$_x$ in the snow at all polar locations considered, and therefore that all NO$_x$ produced by nitrate photolysis from

the snow surface to $3z_e$ escapes from the snow to the atmosphere. The range of F_{NO_x} represents calculations using the full range of observed nitrate concentrations (Dibb et al., 2004, 2007; Frey et al., 2009; Rothlisberger et al., 2000). These results are an upper limit for the flux of NO$_x$ from the snow because we have assumed that all nitrate in the snow is available for photolysis, and that all of the NO$_x$ produced escapes from the snowpack to the overlying atmosphere. Our calculations are compared to observations in the vicinity (< 5 km) of each station. The NO$_x$ fluxes calculated in this study are in good agreement with observed NO$_x$ fluxes estimated near the station at South Pole (Oncly et al., 2004) and observed near the station Dome C (Frey et al., 2013). Oncley et al. (2004) estimated NO$_x$ fluxes using observed NO fluxes together with calculated photochemical equilibrium values for NO$_2$.

The vertical r_e profile (Gallet et al., 2011) is the same for all snowpacks considered in the study, and therefore the concentration of impurities and NO$_3^-$ in the snow influence our calculated flux of NO$_x$ from the snowpack most significantly. The NO$_x$ fluxes from snowpacks greater than 11 km from the station are 1.4–2.3 times larger than the NO$_x$ fluxes from snowpacks near the stations at South Pole and Dome C because near-station snowpacks have higher concentrations of impurities, resulting in shallower e-folding depths. Shallower z_e values near stations confine photodenitrification to a shallower layer, resulting in less NO$_x$ produced (and transported to the atmosphere) compared to remote snowpacks. Here we assume that the snowpack [NO$_3^-$] at South Pole, Dome C, and Summit is the same for each station regardless of distance from the station. The range of F_{NO_x} at each location represents the difference between minimum and maximum observed snowpack [NO$_3^-$].

The contributions from the top 2 cm of snowpack to the total F_{NO_x} varies between stations (24–68 %), but are generally greater in snowpacks near the stations because of shallower e-folding depths of actinic flux. We expect the photodenitrification occurring in the top 2 cm of snow to significantly influence F_{NO_x} because $I_o(\lambda,z)$ and [NO$_3^-$] are greatest in that layer. Although the snowpack [NO$_3^-$] is roughly 3 times higher in the top 2 cm at South Pole and Dome C compared to Summit, Summit has the highest snowpack [NO$_3^-$] below 2 cm and therefore yields the largest overall flux of NO$_x$. Although remote South Pole snowpack has lower [NO$_3^-$] compared to Summit, remote South Pole snowpack yields the second highest F_{NO_x} because it has the largest e-folding depth due to low impurity concentrations. The snowpack [NO$_3^-$] and the e-folding depth of actinic flux influence F_{NO_x} comparably, which can lead to compensating effects. For example, the minimum F_{NO_x} from snowpacks near the stations at South Pole and Dome C are similar because South Pole has higher [NO$_3^-$] but Dome C has a larger e-folding depth. In general, the highest F_{NO_x} results from high snowpack [NO$_3^-$] and large e-folding depths.

4   Conclusions

Observations of the absorption properties of black carbon and non-black carbon material (e.g., brown carbon, dust, organics) in snow collected near Dome C, Antarctica, and Summit, Greenland, show that near-station activities enhance the concentration of absorbing impurities by a factor of at least 2–3, and that the concentrations of absorbing impurities are a factor of 2.5–5 higher at remote locations in Greenland compared to remote locations in East Antarctica. The Ångström exponents associated with the absorption of particulate matter in snow range from 2.3–3 and indicate a combination of black carbon and non-black carbon material in all snow sampled, the latter of which provides the dominant contribution to absorption of UV radiation in the snowpack. The absorption by both BC and nonBC material is increased in near-station snowpacks compared to remote snowpacks. While we cannot quantify the concentration of nonBC (C_{nonBC}), we can infer that the station is a source of both BC and nonBC because the change in the f_{nonBC} is smaller than the change in C_{BC} at increasing distance from the stations. We find that both BC and nonBC concentrations are decreasing away from the station, but that C_{BC} is decreasing at a faster rate compared to C_{nonBC}. Our observations of absorption due to BC and nonBC in snowpack at Dome C, Summit, and South Pole are incorporated into a snowpack actinic flux parameterization.

The parameterization is used to calculate depth-dependent actinic flux profiles in snowpack and is based upon a 4-stream, plane parallel snowpack radiative transfer model with a δ-M approximation (Grenfell, 1991). This parameterization is broadly applicable and allows straightforward inclusion of snowpack properties and impurity types and concentrations. It can be easily implemented into large-scale models and represents spatio-temporal variations in solar zenith angle, wavelength, radiation equivalent ice grain radius, snow density, and impurity concentration. The parameterization was used to calculate actinic flux profiles in snowpack for specific case studies near the stations at Dome C and South Pole and remote from Dome C, South Pole, and Summit. In the UV/near-vis region (the region relevant for photochemistry), the e-folding depth of actinic flux (z_e) is strongly dependent on impurity concentrations (BC and nonBC) and radiation equivalent mean ice grain radius (r_e). z_e decreases with increasing impurity concentration and increases with increasing r_e. Our calculated z_e values range from 8–62 cm between wavelengths of $\lambda = 305$–400 nm; z_e decreases with decreasing wavelength due to the wavelength dependence of nonBC absorption. Our calculated z_e values agree well with previous studies (see Appendix C).

Our results from the parameterization suggest that UV/near-vis radiation is significant at depths greater than 1.5 m in the snowpack, which implies that photodenitrification can occur and produce NO$_x$ at those depths. We calculate the depth dependent lifetime of NO$_x$ in the snow-pack against ventilation to the overlying atmosphere by wind pumping ($\tau_{wind\ pumping}$) and chemical sinks by reaction of NO$_2$ with OH and BrO ($\tau_{chemical}$). Comparison of the vertical profiles of $\tau_{wind\ pumping}$ and $\tau_{chemical}$ at Summit reveals that NO$_x$ is efficiently ventilated to the overlying atmosphere at all depths in the snowpack. This result is sensitive to the assumed concentrations of BrO, snow permeability, viscosity, wind speed, and sastrugi

Our calculated F_{NO_x} near Dome C, South Pole, and Summit range from 3.2×10^8–3.8×10^9 molec cm^{-2} s^{-1} and represent an upper limit on the flux of NO$_x$ from the snow from snowpack nitrate photolysis. Calculated NO$_x$ fluxes in snowpack near stations are a factor of 1.4–2.4 smaller than > 11 km away from the stations due to the impact of absorbing impurity concentrations from local contamination on the e-folding depth of the actinic flux in snowpack. Observations of NO$_x$ fluxes near stations may be underestimating the amount of NO$_x$ emitted from the snowpack in remote locations by a similar factor of 1.4–2.4.

Appendix A

NO$_x$ flux calculation

The flux of NO$_x$ from the snowpack (F_{NO_x}) is calculated for two distinct layers in the snowpack: from the surface ($z = 0$) to z_{ref} (2 cm) and from z_{ref} to three times the e-folding depth ($3z_e$) of actinic flux in snow. These layers are separate because the decay of radiation with depth is in general non-exponential from 0–2 cm and exponential below 2 cm depth. Also, there are significant differences in the vertical profile of snowpack [NO$_3^-$] in the two layers (see Sect. 2.5). The total downwelling irradiance at the snowpack surface is calculated for multiple wavelength bins by the Fast-J radiative transfer program (Wild et al., 2000) with the surface albedo specified to be consistent with our snowpack calculations (0.996). Summations over each λ bin are carried out after depth integrations to ensure that the λ dependence of the e-folding depths are properly included.

In the λ bin ($\lambda_{j+1} - \lambda_j = \Delta\lambda_j$), $I_o(\Delta\lambda_j, z)$ is first calculated at each centimeter in the snowpack from the surface ($z = 0$ cm) to a depth of 3 times the e-folding depth of actinic flux in snow ($3z_e$). Once $I_o(\Delta\lambda_j, z)$ has been calculated at each centimeter, the total (integrated) actinic flux, $\Pi_o(\Delta\lambda_j, \Delta z_i)$, is calculated in a 2 cm interval from $z = 0$ to z_{ref} and 1 cm intervals from $z = z_{ref}$ to $3z_e$ ($z_{i+1} - z_i = \Delta z_i$). Intervals of 1–2 cm are used because IOPs ($c\varpi_{eff}$ and Kext$_{tot}$) vary with depth due to the dependence of grain radius on depth. In each depth interval and wavelength bin, an average

Υ value $\left(\overline{\Upsilon}_{ij} = \left(\overline{c\varpi_{eff}^{\frac{1}{2}}}(\Delta\lambda_j, \Delta z_i) \cdot \overline{\text{Kext}_{tot}}(\Delta\lambda_j, \Delta z_i) \right) \right)$

is used, which uses average values of Kext$_{tot}$ and $c\varpi_{eff}$ over $\Delta\lambda_j$ and each Δz_i. From $z_1 = 0$ to $z_2 = z_{ref}$, $I_o(\Delta\lambda_j, z)$ is numerically integrated over each λ bin ($\Delta\lambda_j$) in the depth

interval ($\Delta z_1 = z_2 - z_1$) using the trapezoid rule.

$$\mathrm{II_o}\left(\Delta\lambda_j, 0\,\mathrm{cm\ to\ 2\,cm}\right) = \frac{\mathrm{I_o}\left(\Delta\lambda_j,\ z_1\right) + \mathrm{I_o}\left(\Delta\lambda_j, z_2\right)}{2}\cdot\Delta z_1 \quad \text{(A1)}$$

Below z_{ref}, $I_o(\Delta\lambda_j, z)$ is analytically integrated over 1 cm intervals (Δz_i).

$$\mathrm{II_o}\left(\Delta\lambda_j, \Delta z_i\right) = \mathrm{I_o}\left(\Delta\lambda_j, z_i\right)\cdot\int_{z_i}^{z_{i+1}} \mathrm{e}^{-\overline{\Upsilon}\cdot z'}\, dz' \quad \text{(A2)}$$

When evaluated, Eq. (A2) becomes

$$\mathrm{II_o}\left(\Delta\lambda_j, \Delta z_i\right) = \mathrm{I_o}(\Delta\lambda_j, z_i)\cdot\left\{\frac{(\mathrm{e}^{-\overline{\Upsilon}\cdot z_i} - \mathrm{e}^{-\overline{\Upsilon}\cdot z_i+1})}{\overline{\Upsilon}}\right\}. \quad \text{(A3)}$$

Values of $\mathrm{II_o}\left(\Delta\lambda_j, \Delta z_i\right)$ calculated in each depth interval (Δz_i) in the $z = z_{\mathrm{ref}}$ to $3z_e$ layer are summed in each λ bin ($\Delta\lambda_j$).

$$\mathrm{II_o}\left(\Delta\lambda_j, 2\,\mathrm{cm\ to\ } 3z_e\right) = \sum_{i=2}^{i=z_{3z_e}} \mathrm{II_o}\left(\Delta\lambda_j, \Delta z_i\right) \quad \text{(A4)}$$

The total flux of NO_x from the snowpack from the layer $z = 0$ to $3z_e$ in each λ bin, $F_{NO_x}(\Delta\lambda_j, 0\,\mathrm{cm\ to\ }3z_e)$, is calculated in Eq. (A5):

$$F_{NO_x}\left(\Delta\lambda_j, 0\,\mathrm{cm\ to\ }3z_e\right) = \overline{\phi}\left(\Delta\lambda_j\right)\cdot\overline{\sigma}\left(\Delta\lambda_j\right)\cdot$$
$$\left(\overline{[NO_3^-]}_{\Delta z_1}\cdot\mathrm{II_o}\left(\Delta\lambda_j, 0\,\mathrm{cm\ to\ 2\,cm}\right) + \overline{[NO_3^-]}_{\Delta z_2\,\mathrm{to\,}\Delta 3z_e}\cdot\right.$$
$$\left.\mathrm{II_o}\left(\Delta\lambda_j, 2\,\mathrm{cm\ to\ }3z_e\right)\right), \quad \text{(A5)}$$

where $\overline{\phi}\left(\Delta\lambda_j\right)$ is the average quantum yield and $\overline{\sigma}\left(\Delta\lambda_j\right)$ is the average absorption cross section in the wavelength bin, $\Delta\lambda_j$. $\overline{[NO_3^-]}_{\Delta z_1}$ is the average snowpack nitrate concentration in the layer from $z = 0$ to z_{ref} and $\overline{[NO_3^-]}_{\Delta z_2\,\mathrm{to\,}\Delta 3z_e}$ is the average snowpack nitrate concentration in the layer from $z = z_{\mathrm{ref}}$ to $3z_e$.

The total flux of NO_x (F_{NO_x}) from the surface snowpack associated with all λ relevant for photodenitrification ($\lambda = 298\text{–}345$ nm) is calculated by summing the total depth-integrated flux of NO_x from the snowpack in each λ bin. Here, 4 λ bins are used consistent with the Fast-J radiative transfer algorithm (Wild et al., 2000) to calculate F_{NO_x} ($N_\lambda = 4$).

$$F_{NO_x} = \sum_{j=1}^{j=N_\lambda} F_{NO_x}\left(\Delta\lambda_j, 0\,\mathrm{cm\ to\ }3z_e\right) \quad \text{(A6)}$$

Appendix B

Dome C and summit filter data

Table B1. Description of individual snow samples collected near Dome C, Antarctica, in January 2004 and Summit, Greenland, in June 2007. The black carbon concentration (C_{BC}), the Angstrom exponent (Å), the fraction of nonBC (f_{nonBC}) absorption in the $\lambda = 650\text{–}700$ nm and $\lambda = 298\text{–}345$ nm ranges, and the snow depths over which these samples were collected are provided.

Distance from station (km)	C_{BC} (ng g^{-1})	Å	$f_{nonBC\_650-700}$ (%)	$f_{nonBC\_298-345}$ (%)	Snow depth (cm)
			Dome C, Antarctica		
11	0.5	3.0	30	0.90	0–20
11	0.6	2.8	28	0.89	0–20
11	0.6	2.9	29	0.89	0–20
11	0.5	2.9	30	0.90	0–20
0.5	0.8	2.5	32	0.91	0–20
1	0.8	2.6	24	0.87	0–20
1.5	0.3	3.4	38	0.93	0–20
2	0.7	2.4	21	0.85	0–20
2.5	0.7	2.5	22	0.85	0–20
3	0.6	2.9	30	0.90	0–20
< 0.5	2.6	2.2	17	0.80	0–3
< 0.5	1.7	2.3	18	0.82	0–3
< 0.5	0.6	3.3	40	0.93	0–20
< 0.5	0.7	2.5	22	0.85	0–20
< 0.5	1.0	2.5	22	0.85	0–20
< 0.5	4.9	2.1	19	0.83	0–3
< 0.5	3.0	2.2	20	0.84	0–3
< 0.5	0.3	3.0	32	0.91	0–3
< 0.5	2.0	2.0	18	0.82	0–3
< 0.5	1.9	1.9	15	0.78	0–3
< 0.5	2.3	2.0	16	0.80	0–3
< 0.5	2.0	2.2	19	0.83	0–3
< 0.5	2.7	2.1	19	0.83	0–3
< 0.5	3.9	2.0	16	0.80	0–3
			Summit, Greenland		
40	1.0	3.0	34	0.91	20–27.5
20	1.4	2.9	31	0.90	20–27.5
20	1.4	2.9	33	0.91	0–7.5
20	1.8	2.2	19	0.83	60–67.5
20	1.5	2.7	27	0.88	80–87.5

Appendix C

Sensitivity of z_e and F_{NO_x} to nonBC absorption

nonBC material dominates absorption in the photochemically active wavelength region. In this study we have used a value of $Å_{nonBC} = 5$ over the λ range 289–850 nm, which results in an exponential dependence of the absorption of nonBC to λ (Doherty et al., 2010, and references within). To examine the sensitivity of z_e and F_{NO_x} to the λ dependence of the absorption of nonBC, we linearly extrapolate Eq. (7) over the UV wavelengths relevant to photochemistry ($\lambda = 289\text{–}345$ nm). We continue to assume $Å_{nonBC} = 5$ (exponential dependence) at λ longer than 345 nm. We find that linear extrapolation of E7 leads to smaller values for the optical depth of nonBC, T_{nonBC}, indicating less absorption of UV radiation due to nonBC material in the snowpack compared to when we assume that $Å_{nonBC} = 5$ in the UV. However, the nonBC absorption is still dominant over BC absorption in

Table D1. e-folding depths measured in snowpacks at Dome C from France et al. (2011) (adapted from Fig. 1).

Snow type	350 nm	400 nm
Soft windpack	$z_e = 9$ cm	$z_e = 10$ cm
Hard windpack	$z_e = 9$ cm	$z_e = 10$ cm
Hoar-like	$z_e = 20$ cm	$z_e = 20$ cm

Table D2. e-folding depths calculated for near-station snowpacks at Dome C using vertical density and radiative equivalent ice grain radius profiles from Gallet et al. (2011).

C_{BC} (ng g^{-1})	ρ_{snow} (g cm^{-3})	r_e (mum)	350 nm	400 nm
1	0.26–0.36	86–460	$z_e = 19$–21 cm	$z_e = 23$–27 cm
3.3			$z_e = 10$–11 cm	$z_e = 13$–15 cm
5			$z_e = 8$–9 cm	$z_e = 10$–12 cm
1	0.26–0.36	61–654	$z_e = 19$–25 cm	$z_e = 27$–32 cm
3.3			$z_e = 10$–11 cm	$z_e = 13$–15 cm
5			$z_e = 8$–10 cm	$z_e = 10$–12 cm
1	0.26–0.36	102–192	$z_e = 16$–19 cm	$z_e = 20$–24 cm
3.3			$z_e = 8$–9 cm	$z_e = 10$–12 cm
5			$z_e = 7$–8 cm	$z_e = 8$–10 cm

the UV ($f_{nonBC\_298-345} = 77$–84 %). When assuming the linear dependence of the absorption of nonBC on λ in the UV, less absorption of UV radiation by nonBC material increases the e-folding depth at $\lambda = 305$ nm by 3–5 cm at all locations except remote South Pole, where the e-folding depth is increased by 10 cm. F_{NO_x} is increased by a factor of 1.1–1.2 depending on location.

Appendix D

Comparison of parameterization to observations and results from other snowpack radiative transfer models

We have compared the measured e-folding depths near the station at Dome C reported in France et al. (2011) to e-folding depths calculated using our actinic flux parameterization. Table D1 (below) shows the e-folding depths measured in France et al. (2011), which have an uncertainty of ± 20 %. We have assumed diffuse sky conditions and used the detailed Dome C snow grain radius and density stratigraphy from Gallet et al. (2011). We have used the average density profile measured by Gallet et al. (2011) near Dome C station for all comparisons, because variations in density are considerably smaller than variations in grain size. We calculate the e-folding depth for various snow BC concentrations using three different r_e profiles from Gallet et al. (2011); the mean profile reported and two "extreme" profiles based upon Fig. 4 in Gallet et al. (2011) (see Table D2). During comparison, we vary BC concentrations from 1–5 ng g^{-1} because it is unclear how much BC was in the snow near Dome C station during the measurement period. We specifically cal-

culate the e-folding depth using $C_{BC} = 3.3$ ng g^{-1} because it was the average concentration measured near Dome C station by Warren et al. (2006). For all comparisons, we assume that nonBC material is responsible for 87 % of the absorption at $\lambda = 305$ and 70 % at $\lambda = 400$ nm, which is the f_{nonBC} calculated from our snow samples collected near Dome C station. Using these assumptions, there is good agreement between the measured e-folding depths at Dome C by France et al. (2011) and the e-folding depths calculated using our parameterization for $C_{BC} = 3.3$–5 ng g^{-1}.

Table D3 compares the normalized actinic flux profile calculated using our parameterization and the normalized actinic flux profiles at Summit, Greenland, calculated with a Monte Carlo radiative transfer model described in Peterson et al. (2002) for a homogenous snowpack with $\rho_{snow} = 340$ kg m^{-3} and snow grain thickness (diameter) $= 0.25$ mm. Table D4 compares the normalized actinic flux profiles for a stratified snowpack with ρ_{snow} ranging from 260–390 kg m^{-3} and snow grain thickness (diameter) ranging from 0.15–0.3 mm. Because the Monte Carlo model does not include snowpack impurities, we have set the impurities in our parameterization to zero. There is good agreement (within 20 %) between the Monte Carlo model and our parameterization for both homogenous and heterogeneous snowpacks.

Table D5 compares the nitrate photolysis rates calculated by Qiu et al. (2002) to our calculated nitrate photolysis rates. Qiu et al. (2002) calculates nitrate photolysis rates based upon chemical actiniometry at 305 nm for two-hour periods near noon in mid-June at Summit. For comparison, we multiply actinic flux at Summit in mid-June from GEOS-Chem by quantum yields and absorption cross sections from Qiu et

Table D3. Comparison of snowpack actinic flux profile for Summit, Greenland, using our parameterization and a Monte Carlo radiative transfer model (Peterson et al., 2002) for homogeneous snowpack with $\rho_{\text{snow}} = 340$ kg m^{-3}, snow grain diameter $= 0.25$ mm, $C_{\text{BC}} = 0$ ng g^{-1}, and diffuse sky conditions.

Depth (mm)	290 nm (Monte Carlo)	290 nm (this work)	350 nm (Monte Carlo)	350 nm (this work)	390 nm (Monte Carlo)	390 nm (this work)
0	1	1	1	1	1	1
5	0.94	0.97	0.95	0.97	0.96	0.98
10	0.91	0.94	0.92	0.94	0.93	0.94
20	0.85	0.88	0.92	0.88	0.93	0.89
40	0.74	0.75	0.79	0.77	0.82	0.78
60	0.65	0.65	0.71	0.67	0.75	0.69
80	0.57	0.56	0.63	0.59	0.68	0.61
100	0.50	0.49	0.58	0.52	0.64	0.53
150	0.36	0.34	0.44	0.37	0.50	0.39
200	0.25	0.23	0.32	0.27	0.37	0.28

Table D4. Comparison of snowpack actinic flux profile for Summit, Greenland, using our parameterization and a Monte Carlo radiative transfer model (Peterson et al., 2002) for stratified snowpack with ρ_{snow} ranging from 260–390 kg m^{-3}, snow grain diameter ranging from 0.15-0.30 mm, $C_{\text{BC}} = 0$ ng g^{-1}, and diffuse sky conditions.

Depth (mm)	290 nm (Monte Carlo)	290 nm (this work)	350 nm (Monte Carlo)	350 nm (this work)	390 nm (Monte Carlo)	390 nm (this work)
0	1	1	1	1	1	1
5	0.94	0.95	0.95	0.96	0.96	0.96
10	0.91	0.90	0.92	0.90	0.93	0.91
20	0.85	0.87	0.92	0.88	0.93	0.89
40	0.74	0.75	0.79	0.77	0.82	0.78
60	0.65	0.65	0.71	0.67	0.75	0.69
80	0.57	0.56	0.63	0.59	0.68	0.61
100	0.50	0.49	0.58	0.52	0.64	0.53
150	0.36	0.34	0.44	0.37	0.50	0.39
200	0.25	0.23	0.32	0.29	0.37	0.28

Table D4. Noon time, mid-June Summit, Greenland, nitrate photolysis rates calculated in Qiu et al. (2002) compared to nitrate photolysis rates calculated using our parameterization.

Depth (cm)	$j(10^{-7}$ s$^{-1})$, Qiu et al. (2002)	$j(10^{-7}$ s$^{-1})$, our parameterization
0	16	14
4	15	11
4	9	10
6	7	9.1
9	6.5	7.5
12	5	6.3
15	7	5.7
20	3	4.1
25	2	2.8

al. (2002) to calculate the nitrate photolysis rate at various depths in the snowpack. The measured and calculated photolysis rates agree within 29 %.

in the snow, and Charlie Zender for information about the optical properties of dust.

Edited by: L. Ganzeveld

References

Albert, M. R. and Hawley, R. L.: Seasonal changes in snow surface roughness characteristics at Summit, Greenland: implications for snow and firn ventilation. Ann. Glaciol., 35, 510–514, 2002.

Albert, M. R. and Shultz, E. F.: Snow and firn properties and air-snow transport processes at Summit, Greenland. Atmos. Environ., 36, 2789–2797, 2002.

Aristidi, E., Agabi, K., Azouit, M., Fossat, E., Vernin, J., Travouillion, T., Lawrence, J. S., Meyer, C., Storey, J. W. V., Halter, B., Roth, W. L., and Walden, V.: An analysis of temperatures and wind speeds above Dome C, Antarctica, Astron. Astrophys., 430, 739–746, 2005.

Beine, H. J., Honrath, R. E., Domine, F., Simpson, W. R., and Fuentes, J. D.: NO$_x$ during background and ozone depletion periods at Alert: Fluxes above the snow surface. J. Geophys. Res., 107, 4584, doi:10.1029/2002JD002082, 2002.

Bey, I., Jacob, D. J., Yantosca, R. M., Logan, J. A., Field, B. D., Fiore, A. M., Li, Q., Liu, H. Y., Mickley, L. J., and Schultz, M. G.: Global modeling of tropospheric chemistry with assimilated meteorology: Model description and evaluation. J. Geophys. Res., 106, 23073–23095, 2001.

Beyersdorf, A. J., Blake, N. J., Swanson, A. L., Meinardi, S., Dibb, J. E., Sjostedt, S., Huey, G., Lefer, B., Rowland, S. F., and Blake, D. R.: Hydroxyl concentrations estimates in the sunlit snowpack at Summit, Greenland. Atmos. Environ., 41, 5101–5109, 2007.

Blunier, T., Gregoire, F. L., Jacobi, H.-W., and Quansah, E.: Isotopic view on nitrate loss in Antarctic surface snow. Geophys. Res. Lett., 32, L13501, doi:10.1029/2005GL023011, 2005.

Bohren, C. F. and Barkstrom, B. R.: Theory of the Optical Properties of Snow, J. Geophys. Res., 79, 4527–4535, doi:10.1029/JC079i030p04527, 1974.

Boxe, C. S., Colussi, A. J., Hoffmann, M. R., Murphy, J. G., Wooldridge, P. J., Bertram, T. H., and Cohen, R. C.: Photochemical Production and Release of Gaseous NO$_2$ from Nitrate-Doped Water Ice. J. Phys. Chem., 109, 8520–8525, 2005.

Boxe, C. S. and Saiz-Lopez, A.: Multiphase modeling of nitrate photochemistry in the quasi-liquid layer (QLL): implications for NOx release from the Arctic and coastal Antarctic snowpack, Atmos. Chem. Phys., 8, 4855–4864, doi:10.5194/acp-8-4855-2008, 2008.

Burkholder, J. B., Ravishankara, A. R., and Solomon, S.: UV/visible and IR absorption cross sections of BrONO$_2$, J. Geophys. Res., 100, 16793–16800, 1995.

Carmagnola, C. M., Domine, F., Dumont, M., Wright, P., Strellis, B., Bergin, M., Dibb, J., Picard, G., and Morin, S.: Snow spectral albedo at Summit, Greenland: comparison between in situ measurements and numerical simulations using measured physical and chemical properties of the snowpack, The Cryosphere Discuss., 6, 5119–5167, doi:10.5194/tcd-6-5119-2012, 2012.

Chen, G., Huey, L. G., Crawford, J. H., Olson, J. R., Hutterli, M. A., Sjostedt, S., Tanner, D., Dibb, J., Lefer, B., Blake, N., Davis, D., and Stohl, A.: An Assesment of the Polar HO$_x$ Photochemical

Budget Based on 2003 Summit Greenland Field Observations, Atmos. Environ., 41, 36, 7806–7820, 2007.

Chu, L. and Anastastio. C.: Quantum Yields of Hydroxyl Radicals and Nitrogen Dioxide from the Photolysis of Nitrate on Ice, J. Phys. Chem., 107, 9594–9602, 2003.

Cotter, E. S. N., Jones, A. E., Wolff, E. W., and Bauguitte, S. J.-B.: What controls photochemical NO and NO$_2$ production from Antarctic snow? Laboratory investigation assessing the wavelength and temperature dependence, J. Geophys. Res., 108, 4147, doi:10.1029/2002JD002602, 2003.

Davis, D., Nowak, J. B., Chen, G., Buhr, M., Arimoto, R., Hogan, A., Eisele, F., Mauldin, L., Tanner, D., Shetter, R., Lefer, B., and McMurry, P.: Unexpected High Levels of NO Observed at South Pole, Geophys. Res. Lett., 28, 3625–3628, 2001.

Davis, D., Chen, G., Buhr, M., Crawford, J., Lenschow, D., Lefer, B., Shetter, R., Eisele, F., Mauldin, L., and Hogan, A.: South Pole NO$_x$ Chemistry: an assessment of factors controlling variability and absolute levels, Atmos. Environ., 38, 5375–5388, 2004.

Davis, D. D., Seelig, J., Huey, G., Crawford, J., Chen, G., Wang, Y., Buhr, M., Helmig, D., Neff, W., Blake, D., Arimoto, R., and Eisele, F.: A reassessment of Antarctic plateau reactive nitrogen based on ANTCI 2003 airborne and ground based measurements. Atmos. Environ., 42, 2831–2848, doi:10.1016/j.atmosenv.2007.07.039, 2008.

Dibb, J. E. and Fahnestock, M.: Snow accumulation, surface height change, and firn densification at Summit, Greenland: Insights from 2 years of in situ observation, J. Geophys. Res., 109, D24113, doi:10.1029/2003JD004300, 2004.

Dibb, J. E., Arsenault, M., Peterson, M. C., and Honrath, R. E.: Fast nitrogen oxide photochemistry in Summer, Greenland snow. Atmos. Environ., 36, 2501–2511, 2002.

Dibb, J. E., Huey, G. L., Slusher, D. L., and Tanner, D. J.: Soluble reactive nitrogen oxides at South Pole during ISCAT 2000. Atmos. Environ., 38, 5399–5409, 2004.

Dibb, J. E., Whitlow, S. I., and Arsenault, M.: Seasonal variations in the soluble ion content of snow at Summit, Greenland: Constraints from three years of daily surface snow samples. Atmos. Environ., 41, 5007–5019, 2007.

Dibb, J. E., Ziemba, L. D., Luxford, J., and Beckman, P.: Bromide and other ions in the snow, firn air, and atmospheric boundary layer at Summit during GSHOX, Atmos. Chem. Phys., 10, 9931–9942, doi:10.5194/acp-10-9931-2010, 2010.

Doherty, S. J., Warren, S. G., Grenfell, T. C., Clarke, A. D., and Brandt, R. E.: Light-absorbing impurities in Arctic snow. Atmos. Chem. Phys., 10, 11647–11680, doi:10.5194/acp-10-11647-2010, 2010.

Domine, F. and Shepson, P. B.: Air-snow interactions and atmospheric chemistry, Science, 297, 1506–1510, 2002.

Dubowski, Y., Colussi, A. J., and Hoffmann, M. R.: Nitrogen Dioxide Release in the 302 nm Band Photolysis of Spray-Frozen Aqueous Nitrate Solutions. Atmospheric Implications. J. Phys. Chem. A, 105, 4928–4932, 2001.

Erbland, J., Vicars, W. C., Savarino, J., Morin, S., Frey, M. M., Frosini, D., Vince, E., and Martins, J. M. F.: Air-snow transfer of nitrate on the East Antarctic Plateau – Part 1: Isotopic evidence for a photolytically driven dynamic equilibrium. Atmos. Chem. Phys. Discuss., 12, 28559–28608, doi:10.5194/acpd-12-28559-2012, 2012.

France, J. L., King, M. D., and Lee-Taylor, J.: The importance of considering depth-resolved photochemistry in snow: a radiative-transfer study of NO$_2$ and OH production in Ny-Alesund (Svalbard) snowpacks, J. Glaciol., 56, 655-663, 2010.

France, J. L., King, M. D., Frey, M. M., Erbland, J., Picard, G., Preunkert, S., MacArthur, A., and Savarino, J.: Snow optical properties at Dome C (Concordia), Antarctica; implications for snow emissions and snow chemistry of reactive nitrogen, Atmos. Chem. Phys., 11, 9787–9801, doi:10.5194/acp-11-9787-2011, 2011.

France, J. L., Reay, H. J., King, M. D., Voisin, D., Jacobi, H.-W., Domine, F., Beine, H. J., Anastasio, C., MacArthur, A., and Lee-Taylor, J.: Hydroxyl radical and NOx production rates, black carbon concentrations and light-absorbing impurities in snow from field measurements of light penetration and nadir reflectivity of on-shore and off-shore coastal Alaskan snow, J. Geophys. Res., 117, D00R12, doi:10.1029/2011JD016639, 2012.

Frey, M. M., Savarino, J., Morin, S., Erbland, J., and Martins, J. M. F.: Photolysis imprint in the nitrate stable isotope signal in snow and atmosphere of East Antarctica and implications for reactive nitrogen cycling, Atmos. Chem. Phys., 9, 8681–8696, doi:10.5194/acp-9-8681-2009, 2009.

Frey, M. M., Brough, N., France, J. L, Anderson, P. S., Traulle, O., King, M. D., Jones, A. E., Wolff, E. W., and Savarino, J.: The diurnal variability of atmospheric nitrogen oxides (NO and NO$_2$) above the Antarctic Plateau driven by atmospheric stability and snow emissions, Atmos. Chem. Phys., 13, 3045–3062, doi:10.5194/acp-13-3045-2013, 2013.

Frieß, U., Deutschmann, T., Gilfedder, B. S., Weller, R., and Platt, U.: Iodine monoxide in the Antarctic snowpack, Atmos. Chem. Phys., 10, 2439–2456, doi:10.5194/acp-10-2439-2010, 2010.

Gallet, J.-C., Domine, F., Arnaud, L., Picard, G., and Savarino, J.: Vertical profiles of the specific surface area and density of the snow at Dome C and on a transect to Dumont D'Urville, Antarctica – albedo calculations and comparison to remote sensing products. The Cryosphere., 5, 631–649, doi:10.5194/tc-5-631-2011, 2011.

Gardiner, B. G. and Martin, T. J.: On measuring and modelling ultraviolet spectral irradiance. Current problems in atmospheric radiation, edited by: Smith, W. L., and Stamnes, K. Adarsh Deepak Publishing, 917–920, 1997.

Grannas, A. M., Jones, A. E., Dibb, J., Ammann, M., Anastasio, C., Beine, H. J., Bergin, M., Bottenheim, J., Boxe, C. S., Carver, G., Chen, G., Crawford, J. H., Dominé, F., Frey, M. M., Guzmán, M. I., Heard, D. E., Helmig, D., Hoffmann, M. R., Honrath, R. E., Huey, L. G., Hutterli, M., Jacobi, H. W., Klán, P., Lefer, B., McConnell, J., Plane, J., Sander, R., Savarino, J., Shepson, P. B., Simpson, W. R., Sodeau, J. R., von Glasow, R., Weller, R., Wolff, E. W., and Zhu, T.: An overview of snow photochemistry: evidence, mechanisms and impacts, Atmos. Chem. Phys., 7, 4329–4373, doi:10.5194/acp-7-4329-2007, 2007.

Grenfell, T. C.: A Radiative Transfer Model for Sea Ice With Vertical Structure Variations. J. Geophys. Res., 96, 16991–17001, 1991.

Grenfell, T. C., Warren, S. G., and Mullen, P. C.: Reflection of solar radiation by the Antarctic snow surface at ultraviolet, visible, and near-infrared wavelength, J. Geophys. Res., 99, 18669–18684, 1994.

Hagler, G. S. W., Bergin, M. H., Smith, E. A., Town, M., Dibb, J. E.: Local anthropogenic impact on particulate elemental carbon concentrations at Summit, Greenland. Atmos. Chem. Phys., 8, 2485–2491, doi:10.5194/acp-8-2485-2008, 2008.

Hansen, J. E. and Travis, L. D.: Light Scattering in Planetary Atmospheres. Space Sci. Rev., 16, 527–610, 1974.

Hoffer, A., Gelencser, A., Guyon, P., Kiss, G., Schmid, O., Frank, G. P., Artaxo, P., Andreae, M. O.: Optical properties of humic-like substances (HULIS) in biomass-burning aerosols, Atmos. Chem. Phys., 6, 3563–3570, doi:10.5194/acp-6-3563-2006, 2006.

Honrath, R. E., Peterson, M. C., Guo, S., Dibb, J. E., Shepson, P. B., and Campbell, B.: Evidence of NO$_x$ production within or upon ice particles in the Greenland snowpack, Geophys. Res. Lett., 26, 695–698, 1999.

Honrath, R. E., Lu, Y., Peterson, M. C., Dibb, J. E., Arsenault, M. A., Cullen, N. J., and Steffen, K.: Vertical fluxes of NO$_x$, HONO, and HNO$_3$ above the snowpack at Summit, Greenland. Atmos. Environ., 36, 2629–2640, 2002.

Jacob, D. J., Heikes, B. G., Fan, S.-M., Logan, J. A., Mauzerall, D. L., Bradshaw, J. D., Singh, H. B., Gregory, G. L., Talbot, R. W., Blake, D. R., and Sachse, G. W.: Origin of ozone and NO$_x$ in the tropical troposphere: A photochemical analysis of aircraft observations over the South Atlantic basin, J. Geophys. Res., 101, 24235–24250, 1996.

Johnston, H. and Graham, R.: Gas-Phase Ultraviolet Absorption Spectrum of Nitric Acid Vapor, J. Phys. Chem., 77, 62–63, 1973.

Jones, A. E., Weller, R., Anderson, P. S., Jacobi, H.-W., Wolff, E. W., Schrems, O., and Miller, H.: Measurements of NO$_x$ emissions from the Antarctic snowpack, Geophys. Res. Lett., 28, 1499–1502, 2001.

Jones, A. E., Wolff, E. W., Ames, D., Bauguitte, S. J.-B., Clemitshaw, K. C., Fleming, Z., Mills, G. P., Saiz-Lopez, A., Salmon, R. A., Sturges, W. T., and Worton, D. R.: The multi-seasonal NOy budget in coastal Antarctica and its link with surface snow and ice core nitrate: results from the CHABLIS campaign, Atmos. Chem. Phys., 11, 9271–9285, doi:10.5194/acp-11-9271-2011, 2011.

Kirchstetter, T. W., Novakov, T., and Hobbs, P. V.: Evidence that the spectral dependence of light absorption by aerosols is affected by organic carbon, J. Geophys. Res., 109, D21208, doi:10.1029/2004JD004999, 2004.

Lamarque, J.-F., McConnell, J. R., Shindell, D. T., Orlando, J. J., and Tyndall, G. S.: Understanding the drivers for the 20th century change of hydrogen peroxide in Antarctic ice-cores, Geophys. Res. Lett., 38, L04810, doi:10.1029/2010GL045992, 2011.

Mauldin, R., Kosciuch, E., Eisele, F., Huey, G., Tanner, D., Sjostedt, S., Blake, D., Chen, G., Crawford, J., and Davis, D.: South Pole Antarctica observations and modeling results: New insights on HO$_x$ radical and sulfur chemistry, Atmos. Environ., 44, 572–581, 2010.

Mayewski, P. A. and Legrand, M. R.: Recent increase in nitrate concentration of Antarctic snow. Nature, 346, 258–260, 1990.

Michalowski, B. A., Francisco, J. S., Li, S.-M., Barrie, L. A., Bottenheim, J. W., and Shepson, P. B.: A computer model study of multiphase chemistry in the Arctic boundary layer during polar sunrise. J. Geophys. Res., 105, 15131–15145, 2000.

Mulvaney, R., Wagenbach, D., and Wolff, E. W.: Postdepositional change in snowpack nitrate from observation of year-round near-surface snow in coastal Antarctica, J. Geophys. Res., 103,

11021–11031, 1998.

Oncley, S. P., Buhr, M., Lenschow, D. H., Davis, D., and Semmer, S. R.: Observations of summertime NO fluxes and boundary-layer height at the South Pole during ISCAT 2000 using scalar similarity. Atmos. Environ., 38, 5389–5398, 2004.

Orvig, S.: Climate of the Polar regions. World survey of climatology, 14, Elsevier, 80–85, 1970.

Peterson, M., Barber, D., and Green, S.: Monte Carlo modeling and measurements of actinic flux levels in Summit, Greenland snowpack, Atmos. Environ., 36, 2545–2551, 2002.

Pinzer, B. R., Kerbrat, M., Huthwelker, T., Gaggeler, H.W., Schneebeli, M., and Ammann, M.: Diffusion of NO$_x$ and HONO in snow: A laboratory study. J. Geophys. Res., 115, doi:10.1029/2009JD012459, 2010.

Qiu, R., Green, S. A., Honrath, R. E., Peterson, M. C., Lu, Y., and Dziobak, M.: Measurements of JNO$_3^-$ in snow by nitrate-based actinometry. Atmos. Environ., 36, 2563–2571, 2002.

Roden, C. H., Bond, T. C., Conway, S., and Osorto Pinel, A. B.: Emission factors and real-time optical properties of particles emitted from traditional wood burning cookstove. Environ. Sci. Technol., 40, 6750–6757, 2006.

Rothlisberger, R., Hutterli, M. A., Sommer, S., Wolff, E. W., and Mulvaney, R.: Factors controlling nitrate in ice cores: Evidence from the Dome C deep ice core. J. Geophys. Res., 105, 20565–20572, 2000.

Saiz-Lopez, A., Plane, J. M. C., Mahajan, A. S., Anderson, P. S., Bauguitte, S. J.-B., Jones, A. E., Roscoe, H. K., Salmon, R. A., Bloss, W. J., Lee, J. D., and Heard, D. E.: On the vertical distribution of boundary layer halogens over coastal Antarctica: implications for O$_3$, HO$_x$, NO$_x$ and the Hg lifetime, Atmos. Chem. Phys., 8, 887–900, doi:10.5194/acp-8-887-2008, 2008.

Sander, S. P., Friedl, R. R., Golden, D. M., Kurylo, M. J., Moortgat, G. K., Keller-Rudek, H., Wine, P. H., Ravishankara, A. R., Kolb, C. E., Molina, M. J., Finlayson-Pitts, B. J., Huie, R. E., and Orkin, V. L.: Chemical Kinetics and Photochemical Data for Use in Atmospheric Studies Evaluation Number 15. JPL Publication, 06-2, 2006.

Savarino, J., Kaiser, J., Morin, S., Sigman, D. M., and Thiemens, M. H.: Nitrogen and oxygen isotopic constraints on the origin of atmospheric nitrate in coastal Antarctica, Atmos. Chem. Phys., 7, 1925–1945, doi:10.5194/acp-7-1925-2007, 2007.

Seinfeld, J. H. and Pandis, S. N.: Atmospheric Chemistry and Physics From Air Pollution to Climate Change, John Wiley & Sons Inc., p. 224, 1998.

Sjostedt, S. J., Huey, L. G., Tanner, D. J., Peischl, J., Chen, G., Dibb, J. E., Lefer, B., Hutterli, M. A., Beyersdorf, A. J., Blake, N. J., Blake, D. R., Sueper, D., Ryerson, T., Burkhart, J., and Stohl, A.: Observations of hydroxyl and the sum of peroxy radicals at Summit, Greenland during summer 2003, Atmos. Environ., 41, 5122–5137, 2007.

Slusher, D. L., Huey, L. G., Tanner, D. J., Chen, G., Davis, D. D., Buhr, M., Nowak, J. B., Eisele, F. L., Kosciuch, E., Mauldin, R. L., Lefer, B. L., Shetter, R. E., and Dibb, J. E.: Measurements of pernitric acid at the South Pole during ISCAT 2000, Geophys. Res. Lett., 29, 2011, doi:10.1029/2002GL015703, 2002.

Stamnes, K., Tsay, S., Wiscome, and Jayaweera, W.: Numerically stable algorithm for discrete-ordinate-method radiative transfer in multiple scattering and emitting layered media. Appl. Opt., 27, 2502–2509, 1988.

Steffen, K. and Box, J.: Surface climatology of the Greenland ice sheet: Greenland Climate Network 1995–1999, J. Geophys. Res., 106, 33951–33964, 2001.

Stutz, J., Thomas, J. L., Hurlock, S. C., Schneider, M., von Glasow, R., Piot, M., Gorham, K., Burkhart, J. F., Ziemba, L., Dibb, J. E., and Lefer, B. L.: Longpath DOAS observations of surface BrO at Summit, Greenland, Atmos. Chem. Phys., 11, 9899–9910, doi:10.5194/acp-11-9899-2011, 2011.

Thomas, J. L., Stutz, J., Lefer, B., Huey, L. G., Toyota, K., Dibb, J. E., and von Glasow, R.: Modeling chemistry in and above snow at Summit, Greenland – Part 1: Model description and results. Atmos. Chem. Phys., 11, 4899–4914, doi:10.5194/acp-11-4899-2011, 2011.

Thomas, J. L., Dibb, J. E., Huey, L. G., Liao, J., Tanner, J., Lefer, B., von Glasow, R., and Stutz, J.: Modeling chemistry in and above snow at Summit, Greenland – Part 2: Impact of snowpack chemistry on the oxidation capacity of the boundary layer, Atmos. Chem. Phys., 12, 6537–6554, doi:10.5194/acp-12-6537-2012, 2012.

Tie, X., Zhang, R., Brasseur, G., Emmons, L., and Lei, W.: Effects of lightning on reactive nitrogen and nitrogen reservoir species in the troposphere. J. Geophys. Res., 106, 3167–3178, 2001.

Voisin, D., Jafferzo, J. L., Houdier, S., Barret, M., Cozic, J., King, M. D., France, J. L., Reay, H. J., Grannas, A., Kos, G., Ariya, P. A., Beine, H. J., and Domine, F.: Carbonaceous species and humic like substances (HULIS) in Arctic snowpack during OASIS field campaign in Barrow. J. Geophys. Res., 117, D00R19, doi:10.1029/2011JD016612, 2012.

Waddington, E. D., Cunningham, J., and Harder, S. L.: The effects of snow ventilation on chemical concentrations. NATO ASI Series, I 43, 404–451, 1996.

Wang, Y., Choi, Y., Zeng, T., Davis, D., Buhr, M., Huey, G. L., and Neff, W.: Assessing the photochemical impact of snow NO$_x$ emissions over Antarctica during ANTCI 2003, Atmos. Environ., 41, 3944–3958, doi:10.1016/j.atmosenv.2007.01.056, 2007.

Warneck, P. and Wurzinger, C.: Product Quantum Yields for the 305-nm Photodecomposition of NO$_3^-$ In Aqueous Solution, J. Phys. Chem., 92, 6278–6283, doi:10.1021/j00333a022, 1988.

Warren, S. G. and Brandt, R. E.: Optical constants of ice from the ultraviolet to the microwave: A revised compilation, J. Geophys. Res., 113, D14220, doi:10.1029/2007jd009744, 2008.

Warren, S. G. and Clarke, A. D.: Soot in the Atmosphere and Snow Surface of Antarctica, J. Geophys. Res., 95, 1811–1816, 1990.

Warren, S. G., Brandt, R. E., and Hinton, P.-O.: Effect of surface roughness on bidirectional reflectance of Antarctic snow. J. Geophys. Res., 103, 25789–25807, 1998.

Warren, S. G., Brandt, R. E., and Grenfell, T. C.: Visible and near-ultraviolet absorption spectrum of ice from transmission of solar radiation into snow, Appl. Opt., 45, 5320–5334, 2006.

Wild, O., Zhu, X., and Prather, M. J.: Fast-J: Accurate Simulation of In- and Below-Cloud Photolysis in Tropospheric Chemical Models, J. Atmos. Chem., 37, 245–282, 2000.

Wiscombe, W. J.: The Delta-M method: Rapid Yet Accurate Radiative Flux Calculations for Strongly Asymmetric Phase Functions. J. Atmos. Sci., 34, 1408–1422, 1977.

Wiscombe, W. J. and Warren, S. G.: A Model for the Spectral Albedo of Snow – I: Pure Snow, J. Atmos. Sci., 37, 2712–2733, 1980.

Wolff, E. W., Jones, A. E., Martin, T. J., and Grenfell, T. C.: Modelling photochemical NO$_x$ production and nitrate loss in the upper snowpack of Antarctica. Geophys. Res. Lett., 29, 1944, doi:10.1029/2002GL015823, 2002.

Yang, X., Cox, R. A., Warwick, N. J., Pyle, J. A., Carver, G. D., O'Connor, F. M., and Savage, N. H.: Tropospheric bromine chemistry and its impacts on ozone: A model study. J. Geophys. Res., 110, D23311, doi:10.1029/2005JD006244, 2005.

Zender, C. S., Bian, H., and Newman, D.: The mineral dust entrainment and deposition (DEAD) model: description and 1990s dust climatology, J. Geophys. Res., 108, 4416, doi:10.1029/2002JD002775, 2003.